Euro. Jnl of Applied Mathematics (2015), *vol.* 26, *pp.* 355–382.
doi:10.1017/S0956792515000066

Interface closure in the root region of steady deep-cellular growth in directional solidification

J.-J. XU[1,2] and Y.-Q. CHEN[3]

[1]*School of Material Science and Engineering, USTB, Beijing, 100083, China*
email: xu@math.mcgill.ca
[2]*Department of Mathematics and Statistics, McGill University, Montreal, Quebec, H3A 0B9, Canada*
[3]*School of Science, Tianjin Chengjian University, Tianjin, 300384, China*
email: yonqiang@gmail.com

(*Received 2 November 2013; revised 29 January 2015; accepted 3 February 2015; first published online 6 March 2015*)

The present paper investigates the mechanism of interface closure in the root region of the solutions for steady deep-cellular growth. This phenomenon is determined by a transcendentally small factor beyond all orders. It is found that the root region comprises three inner-inner regions; the inner system in the root region has a simple turning point, whose presence generates the so-called *trapped-waves mechanism*, which is responsible for the interface closure at the bottom of root. The quantization condition derived from the trapped-waves mechanism yields the eigenvalue that determines the location of interface closure and its dependence on the interfacial energy and other physical parameters.

Key words: Asymptotics beyond all orders; Multiple variables expansion; Quantization condition; Steady deep-cellular growth; Interface closure

1 Introduction

Steady deep-cellular growth for a system of binary mixture in directional solidification has been a subject of focused study in condensed matter physics and material science for decades [1–10]. The profound understanding of the interfacial pattern formation in the system of deep-cellular growth has great significance not only theoretically in condensed matters physics, but also practically in applications of material processing industries. There have been many experimental investigations and numerical simulations on this subject by using a model device – the Hele-Shaw cell, which consists of a thin sample of binary material and two uniform temperature zones: a hot zone with a temperature T_{H} higher than the melting temperature T_{M0} of a flat interface and a cold zone with a temperature T_{C} lower than the melting temperature. The sample is pulled along the direction from the hot zone to cold zone, with V much greater than the critical number V_c activating the linear Mullins–Sekerka instability. Analytical investigations of deep-cellular growth were relatively few, due to the strong nonlinearity of the mathematical problem involved. Substantial progress was made in the sequence of papers by Xu and his co-worker in recent years (refer to [11, 12]) which developed a global theory for the steady deep-cellular growth and their global stability mechanisms. In [11], by adopting

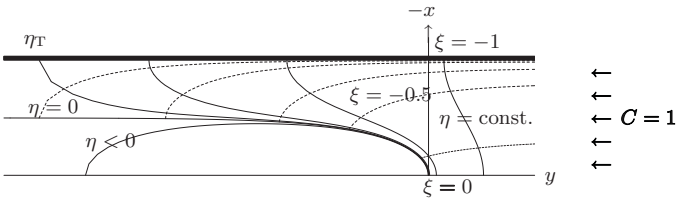

FIGURE 1. The sketch of the orthogonal curvilinear coordinate system (ξ, η) based on the Saffman–Taylor solution.

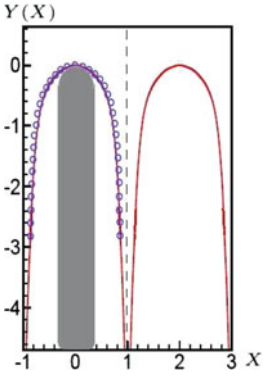

FIGURE 2. The interface shape in the (X, Y) plane calculated by using the first order outer solution derived in [11] for the typical case: $\kappa = 0.29$, $c_\infty = 1.2\,\text{mol}\%$ and the pulling velocity $V = 12\mu\text{m/s}$, the temperature gradient $G_D = 140.0 \times 10^{-4}\text{K}/(\mu\text{m})$, primary spacing $\ell_w = 90\ \mu\text{m}$ and the tip radius $\ell_t = 22.4\mu\text{m}$. The grey area describes the viscous finger given by S–T solution. The circles represent the experimental data obtained by Pocheau et al. [22].

the curvilinear coordinate system (ξ, η) as shown in Figure 1, Chen–Xu showed that the solutions of steady deep-cellular growth can be expanded in the form of the regular perturbation expansion (RPE) in the limit of Péclet number $\epsilon = \text{Pe} \to 0$ while the surface tension parameter $\Gamma = O(\epsilon^2)$. It is obtained that in the zeroth order approximation, the RPE solution of cellular growth reduces to Saffman–Taylor (S–T) solution for the system of viscous fingering in Hele-Shaw flow [13–16], showing that the finger-like interface of the solution extends to infinity without closure. This result recovers the finding by Pelce and Pumir in 1986 [4]. Chen–Xu further derive the analytical form of the first order approximate RPE solution and find that its finger-like interface also extends to infinity without a closure as shown in Figure 2. More importantly, Xu and his co-worker prove that, up to any order approximations $O(\epsilon^N)$, the finger-like interface of the RPE solution still extends to infinity without a closure.

In reality, one prominent feature of the steady deep-cellular growth is that the system forms a long narrow groove and the finger-like interface always has a smooth closure at the bottom. Thus, the RPE solution obtained by Chen–Xu naturally raises the questions, as to what is the mechanism of the interface closure for the steady deep-cellular growth; how to determine the location of the closure and its dependence on the interfacial-energy and other physical parameters.

https://doi.org/10.1017/S0956792515000066 Published online by Cambridge University Press

It is seen that the interface closure observed in the experiments is a phenomenon determined by some transcendentally small pre-factor with the magnitude $\delta(\epsilon) = O\left(e^{-\frac{A}{\epsilon}}\right)$ 'beyond all orders'. The physical phenomena, in which a transcendentally small pre-factor 'beyond all orders' plays crucial role, have been previously encountered and extensively investigated in the areas of nonlinear science, fluid dynamics, and crystal growth (refer to [17–21]). The interface closure in the steady deep-cellular growth is another prominent example on this subject.

It is evident that the transcendentally small term missed by the RPE solution derived in [11] is very hard to 'catch' with the numerical simulations without the analytical treatment. A typical example given in the present paper and described in Figure 12 shows that as $\epsilon = 0.1$, one has $\delta(\epsilon) \approx 0.4 \times 10^{-8}$. The desirable information delivered by such small factor will be fully submerged by the 'numerical noise' generated by the unavoidable rounding-off and truncation errors involved in the numerical simulations.

To demonstrate this argument more clearly, we carry out the numerical computations with different truncation errors for the first order approximate RPE solution obtained in [11] (refer to (32) in that paper). The numerical results are shown in Figure 3(a) and (b), respectively. The solution has been obtained in the closed analytical form, and it has been proven analytically that its interface extends to infinity with no interface closure, while the numerical implementation of this analytical solution exhibits an interface closure due to the numerical truncation errors. Moreover, the calculations with different truncation errors result in different locations of interface closure. The above demonstration casts serious doubt over the results of the numerical simulations with different numerical methods that have shown the interface closure in the system of deep-cellular growth (see, for instance, [6, 7]).

One may conclude that to explore the mechanism of interface closure and its dependence on the physical parameters of the system, the analytical approach is not only preferable, but also necessary.

The issues were investigated in [11], in which the whole physical region was divided into the outer region away from the location of interface closure and the root region near the location of interface closure. Some singular perturbation expansion (SPE) form of solutions in the root region was derived. The elegant multiple-layers structure of the inner solution was explored. Moreover, the work formulated an eigenvalue problem (EVP) for the determination of the location of interface closure. However, the inner equation in the root region derived in [11] was in error, which omitting the important effect of the curviness of the interface in the root region, hence missing the complex turning point existing in the root region – a significant piece for resolving the puzzle. As a consequence, in [11], the critical role of such turning point on the behaviour of the inner solution in the root region was not well explored, and the issues of the mechanism for interface closure and the formation of the multi-layer structure of solution in the root region were still not fully resolved.

The present paper attempts to continue the investigation of these issues. The most important new result that we find is that in the root region, the steady solutions of deep-cellular growth have the multi-layer structure, the inner system of the deep-cellular growth in the root region has a simple turning point $\hat{\xi}_c$ on the extended complex plane, affected by the surface tension and other physical parameters of the system. The

https://doi.org/10.1017/S0956792515000066 Published online by Cambridge University Press

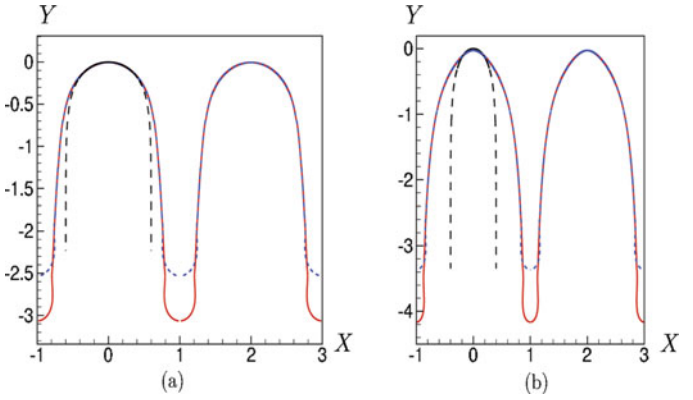

FIGURE 3. The numerical descriptions of the interface shapes computed by using the analytical form of the first order approximate outer solution obtained in [11]. The blue dashed line is calculated by the Fourier cosine series involved truncated at 6,000 terms, while the solid red line is calculated by the Fourier cosine series involved truncated at 60,000 terms for the typical cases $\epsilon = 0.1, \mathbb{M} = 6.0$, $\hat{\Gamma} = 0.3, \kappa = 0.1$, and (a) $\lambda_G = 2.0, \lambda_0 = 0.6$; (b) $\lambda_G = 1.0, \lambda_0 = 0.4$. In both (a) and (b), the black dashed line is given by S–T solution, corresponding to the case of $\epsilon = 0$.

presence of the turning point singularity generates the so-called *trapped-waves mechanism*, which is responsible for the interface closure and leads to the quantization condition for determination of the location of interface closure.

The present paper is arranged as follows. In Section 2, we give the mathematical formulation of the problem and list the form of outer solutions obtained in [11]. In Section 3, we give the mathematical description of inner system in the root region. The interface shape in the root region is divided into sub-region (I) near the bottom of root and subregion (II), the far field of root region, the approximate form of the RPE-part of interface shape solution and its corresponding composite solution are derived. In Section 4, we give the inner system for the form of SPE-part of root solution, and give the general forms of inner-inner solutions in the sub-region (II) and (I), respectively. We further show the existence of the turning point $\hat{\xi}_c$ in the extended complex $\hat{\xi}$-plane. In Section 5, we derive the inner-inner equation in sub-domain (T) near the turning point and reduce the equation into the Airy equation. Furthermore, we derive the turning point solution in sub-domain (T). In Section 6, we match the turning point solution with the inner-inner solutions in the sectors (S_1) and (S_2), which are away from the turning point $\hat{\xi}_c$ and respectively contain the far field of root region and the bottom of root. In Section 7, we derive the quantization condition for the steady state solution by applying the smoothness condition at the bottom of root, elucidate the *trapped-wave mechanism* and show the numerical results for some typical cases. Finally, in Section 8, we summarize the results and draw some conclusions.

2 Mathematical formulation of problem and a brief summary of outer solution

We adopt the model and the notation as adopted in [11], using the tip radius ℓ_t as the length scale and using the dimensional impurity concentration in the far field $(C_\infty)_D$ as

https://doi.org/10.1017/S0956792515000066 Published online by Cambridge University Press

the scale of the concentration. Write W as the half of the primary spacing. As usual, we assume that the temperature in the region where an interfacial microstructure forms is linear with given gradient $(G)_{\mathrm{D}}$; the minor species in the binary mixture, considered as an impurity, is dilute; the solute diffusion in the solid phase is negligible; the thermodynamic properties other than the diffusivity are the same for both solid and liquid phases, and there is no convection in the system.

The solute-diffusion length in the system is defined as $\ell_{\mathrm{D}} = \kappa_{\mathrm{D}}/V$, where κ_{D} is the solute diffusivity. We use the tip radius ℓ_{t} as the length scale and assume that $\ell_{\mathrm{t}} \ll \ell_{\mathrm{D}}$. The pulling speed V is used as the velocity scale, and ℓ_{t}/V is used as the time scale. The scales of the temperature T and concentration C are set as $\Delta H/(c_{\mathrm{p}}\rho)$ and C_∞, respectively. Herein, ΔH is the latent heat release per unit of volume of the solid phase, c_{p} is the specific heat, ρ is the density of the melt and C_∞ is the impurity concentration in the far field. One may define the following dimensionless parameters: the Péclet number, $\epsilon = \ell_{\mathrm{t}}/\ell_{\mathrm{D}}$; the morphological parameter, $\mathbb{M} = -\frac{mC_\infty}{\Delta H/(c_{\mathrm{p}}\rho)}$, where $m < 0$ is the slope of the liquidus in the phase diagram; the surface-tension parameter, $\Gamma = \frac{\ell_{\mathrm{c}}}{\ell_{\mathrm{t}}} = \frac{\ell_{\mathrm{c}}\ell_{\mathrm{D}}}{\ell_{\mathrm{t}}^2}\frac{\ell_{\mathrm{t}}}{\ell_{\mathrm{D}}}$, where ℓ_{c} is the capillary length defined as $\ell_{\mathrm{c}} = \gamma c_{\mathrm{p}}\rho T_{\mathrm{M0}}/(\Delta H)^2$, and γ is the surface-tension coefficient; the dimensionless gradient of the temperature, $\mathrm{G} = \frac{\ell_{\mathrm{D}}}{\Delta H/(c_{\mathrm{p}}\rho)}(G)_{\mathrm{D}}$; the ratio of two length scales, $\lambda_{\mathrm{G}} = \ell_{\mathrm{D}}/\ell_{\mathrm{G}} = \mathrm{G}/\mathbb{M}$, where $\ell_{\mathrm{G}} = -mC_\infty/(G)_{\mathrm{D}}$; the primary spacing parameter, $W = \ell_w/\ell_{\mathrm{t}}$. In most practical cases, the surface-tension parameter is very small, $\Gamma \ll 1$. We assume $\epsilon \ll 1$ and $\Gamma = O(\epsilon^2)$ and, accordingly, set $\Gamma = \epsilon^2\hat{\Gamma}$, where $\hat{\Gamma} = O(1)$.

Due to the periodicity of the solution, we may only consider a single cell. In this case, the problem is equivalent to finger-like crystal growth in a channel with fixed side walls $x = \pm W$.

We, as in [11], formulate the problem in the curvilinear coordinate system (ξ, η) based on the S–T solution for the system of viscous fingering in the form:

$$Z = X + \mathrm{i}Y = Z(\zeta) = \lambda_0\zeta + \mathrm{i}\frac{2(1-\lambda_0)}{\pi}\ln\cos\left(\frac{\pi\zeta}{2}\right), \tag{2.1}$$

where λ_0 is the asymptotic width of finger, $\zeta = \xi + \mathrm{i}\eta$, $X(\xi,\eta) = x/W$, $Y(\xi,\eta) = y/W$. The variables $\{\xi = \xi(X,Y); \eta = \eta(X,Y)\}$ constitute a new orthogonal curvilinear coordinate system on the (X,Y)-plane as shown in Figure 1. The origin of the coordinates is set at a finger-tip.

In the curvilinear coordinate system (ξ, η), the linear distribution of temperature field is described by $T_{\mathrm{B}} = \epsilon\mathrm{G}\big[WY(\xi,\eta) - y_0\big]$.

2.1 Governing equation and boundary conditions

The basic steady-state of cellular growth $\{C_{\mathrm{B}}, \eta_{\mathrm{B}}\}$ is subject to the governing equation:

$$\frac{\partial^2 C_{\mathrm{B}}}{\partial\xi^2} + \frac{\partial^2 C_{\mathrm{B}}}{\partial\eta^2} + \epsilon W\left(Y_\xi\frac{\partial C_{\mathrm{B}}}{\partial\xi} + X_\xi\frac{\partial C_{\mathrm{B}}}{\partial\eta}\right) = 0\,, \tag{2.2}$$

with the following boundary conditions:

(1) In the up-stream far field: far away from cell tips, the effect of micro-structure at

https://doi.org/10.1017/S0956792515000066 Published online by Cambridge University Press

the interface on the concentration distribution field is negligible. Hence, it may be imposed that as $\eta \to \infty$, $C_{\mathrm{B}} \sim 1 + Q_0(\epsilon)\mathrm{e}^{-\epsilon W \eta}$, where $Q_0(\epsilon)$ is a constant, independent of the variables ξ, η.

(2) At the side walls, $\xi = \pm 1$: $\frac{\partial C_{\mathrm{B}}}{\partial \xi} = 0$.

(3) At the interface $\eta = \eta_{\mathrm{B}}(\xi, \epsilon)$,

$$C_{\mathrm{B}} = y_* - \epsilon \lambda_{\mathrm{G}} W Y(\xi, \eta) - \frac{\epsilon^2 \hat{\Gamma}}{\mathbb{M} W} \mathscr{K}\left\{\eta_{\mathrm{B}}(\xi, \epsilon)\right\}, \tag{2.3}$$

$$\frac{\partial C_{\mathrm{B}}}{\partial \eta} - \eta'_{\mathrm{B}} \frac{\partial C_{\mathrm{B}}}{\partial \xi} - \epsilon W (1-\kappa) C_{\mathrm{B}} \left(Y_\xi \eta'_{\mathrm{B}} - Y_\eta\right) = 0, \tag{2.4}$$

where $\mathscr{K}\{\eta_{\mathrm{B}}(\xi, \epsilon)\}$ is the twice mean curvature operator, and we designate that $\mathscr{K} > 0$, **when an interfacial finger points to liquid phase side**, κ is the segregation coefficient, and $\mathbb{M}$ is the morphological number, proportional to the slope m of the liquidus in the phase diagram. We write $y_* = \epsilon \lambda_{\mathrm{G}} y_0$, and assume that $y_* = y_{*0} + \epsilon y_{*1} + \cdots$, as $\epsilon \to 0$.

(4) At the cell tip, $\xi = \eta = 0$: $\frac{\partial \eta_{\mathrm{B}}}{\partial \xi}(0) = \eta_{\mathrm{B}}(0) = 0$.

(5) At the bottom of root, $\xi = \pm 1$, $\eta = \eta_{\mathrm{b}}$: $\eta_{\mathrm{B}}(\pm 1) = \eta_{\mathrm{b}}$; $\frac{\partial \eta_{\mathrm{B}}}{\partial \xi}(\pm 1) = 0$.

2.2 Brief summary of outer solutions

As shown in [11], the whole physical space can be divided into the outer region away from the bottom of the cell and the root region near the bottom of the cell. The outer solution for concentration as $\epsilon \to 0$ has the asymptotic form:

$$\begin{aligned} C_{\mathrm{B}}(\xi, \eta, \epsilon) &\sim \bar{C}_{\mathrm{R}}(\xi, \eta, \epsilon) + \bar{C}_{\mathrm{S}}(\xi, \eta, \epsilon), \\ \eta_{\mathrm{B}}(\xi, \epsilon) &\sim \epsilon \left[\bar{\eta}_{\mathrm{R}}(\xi, \epsilon) + \bar{\eta}_{\mathrm{S}}(\xi, \epsilon)\right]. \end{aligned} \tag{2.5}$$

The first part of solution $\{\bar{C}_{\mathrm{R}}(\xi, \eta, \epsilon), \bar{\eta}_{\mathrm{R}}(\xi, \epsilon)\}$ is called the RPE part, whose asymptotic factors depend on ϵ algebraically, such that $\{\epsilon, \epsilon^2, \epsilon^3, \ldots\}$; the second part of the solution $\{\bar{C}_{\mathrm{S}}(\xi, \eta, \epsilon), \bar{\eta}_{\mathrm{S}}(\xi, \epsilon)\}$ is called the SPE part, whose asymptotic factors depend on ϵ exponentially. It is shown in [11] that the RPE-part of solution has the three distinct features: (i) It contains no free constant; (ii) It violates the interface-tip condition, since $\bar{\eta}_{\mathrm{R}}(0) \neq 0$; (iii) It shows no interface closure, since $\xi \to \pm 1$, $\bar{\eta}_{\mathrm{R}}(\xi) \to 0$. The leading order approximation of RPE-part is obtained in [11]. The RPE solution for the concentration field is

$$\bar{C}_{\mathrm{R}}(\xi, \eta, \epsilon) \approx \bar{C}_0(\xi, \eta, \epsilon) = y_{*0} + \epsilon \left\{y_{*1} - W \lambda_G Y(\xi, \eta) + W\left[\lambda_{\mathrm{G}} - (y_{*0} - 1)\right] \eta\right\}, \tag{2.6}$$

where $y_{*0} = \frac{1+\lambda_{\mathrm{G}}(1-\lambda_0)}{1-\lambda_0(1-\kappa)}$, $y_{*1} = \frac{W(1-\kappa)\lambda_0 \lambda_{\mathrm{G}} \beta_0}{(1-\kappa)\lambda_0 - 1}$ and $\beta_0 = -\frac{2(1-\lambda_0)}{\pi} \ln 2$; $\lambda_0 = \frac{y_{*0} - 1 - \lambda_{\mathrm{G}}}{(1-\kappa) y_{*0} - \lambda_{\mathrm{G}}}$. The asymptotic width parameter λ_0 is connected with the primary spacing parameter W via the formula: $W = \frac{\pi(1-\lambda_0)}{2\lambda_0^2}$.

The leading order approximation of RPE part solution for the interface shape function $\bar{\eta}_{\mathrm{R}}(\xi, \epsilon) \approx \bar{h}_1(\xi)$ is expressed in the form of the Fourier cosine series in [11]. The graph of $\bar{h}_1(\xi)$ for a typical case is shown in Figure 4 on the (ξ, η) plane. It is found that $\bar{h}_1(0) \neq 0$

https://doi.org/10.1017/S0956792515000066 Published online by Cambridge University Press

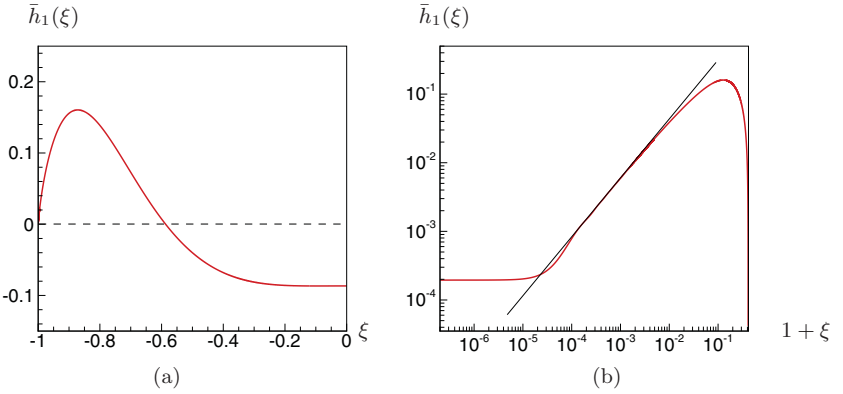

FIGURE 4. The feature of RPE solution $\bar{h}_1(\xi)$ of the outer solution for the case $\epsilon = 0.1, \mathbb{M} = 6.0$, $\hat{\Gamma} = 0.3, \kappa = 0.1$, and $\lambda_G = 2.0, \lambda_0 = 0.6$; (a) The graph of the function $\bar{h}_1(\xi)$ in the outer region; (b) The red line shows the behaviour of the function $\bar{h}_1(\xi)$ near $\xi = -1$ affected by the numerical errors. The black line is the asymptote, $\bar{h}_1 = 2.63(1+\xi)^{0.88}$.

and as $\xi \to -1$, $\bar{h}_1(\xi) \sim \mathfrak{a}_0(\xi+1)^\alpha, (0 < \alpha < 1)$, $\lim_{\xi\to-1} \bar{h}_1(\xi) = 0$. Consequently, the RPE solution violates the interface-tip condition, $\bar{\eta}_B(0) = 0$, and yields an infinitely long finger-like interface in the (X, Y) plane tangent to the line $X = -1$ at $Y = -\infty$ with no interface closure, as indicated before.

In order to satisfy the interface-tip condition $\bar{\eta}_B(0) = 0$, as a consequence, one must introduce the additional SPE part expressed in the form of multiple variables for the outer solution. The leading order approximation of SPE part: $\{\bar{C}_S(\xi,\eta,\epsilon) \sim \bar{\mathfrak{C}}_0(\xi,\eta,\xi_+,\eta_+); \bar{\eta}_S(\xi,\epsilon) \sim \bar{\mathbb{h}}_0(\xi_+)\}$, has the features: (i) It contains some free constants; (ii) It is transcendentally small as $\epsilon \to 0$ for fixed $\xi \neq 0$, namely this is true except at the interface-tip ($\xi = 0$); (iii) It has multiple length scales, so that can be described in the form of multiple variables $\{\xi,\eta,\xi_+,\eta_+\}$, defined as $\xi_+ = 1/\sqrt{\epsilon\hat{\Gamma}}\int_0^\xi k(\xi_1,\eta)\mathrm{d}\xi_1$; $\eta_+ = 1/\sqrt{\epsilon\hat{\Gamma}}\int_0^\eta k(\xi,\eta_1)\mathrm{d}\eta_1$, where $k(\xi,\eta) \sim k_0(\xi,\eta) + \epsilon k_1(\xi,\eta) + \cdots$; (iv) it vanishes exponentially, as $\xi \to \pm 1$.

The leading order approximation of SPE part of solution $\bar{\eta}_S(\xi,\epsilon)$ is obtained in [11] as

$$\bar{\eta}_S(\xi,\epsilon) \approx \bar{\mathbb{h}}_0(\xi_+) = \bar{\mathfrak{d}}_0 \Re\left\{\mathrm{e}^{\frac{1}{\sqrt{\epsilon\hat{\Gamma}}}\chi(\xi)}\right\} = \bar{\mathfrak{d}}_0 \mathrm{e}^{\frac{\chi_I(\xi)}{\sqrt{\epsilon\hat{\Gamma}}}} \cos\left(\frac{\chi_R(\xi)}{\sqrt{\epsilon\hat{\Gamma}}}\right), \tag{2.7}$$

where $\bar{\mathfrak{d}}_0$ is an arbitrary constant,

$$\chi(\xi) = \int_0^\xi \bar{k}_s(\xi_1)\mathrm{d}\xi_1 = \chi_R(\xi) + \mathrm{i}\chi_I(\xi), \tag{2.8}$$

$$\bar{k}_s(\xi) = W\sqrt{\mathbb{M}\Delta_0 \mathscr{G}_0(\xi,0)\left[1 + \frac{\mathrm{i}}{\lambda_0} Y_{\xi,0}(\xi,0)\right]}, \tag{2.9}$$

and $\mathscr{G}_0(\xi,0) \sim -(1-\lambda_0)\tan\left(\frac{\pi\xi}{2}\right)$, $Y_{\xi,0}(\xi,0) = -(1-\lambda_0)\tan(\frac{\pi\xi}{2})$. It is seen that by setting

https://doi.org/10.1017/S0956792515000066 Published online by Cambridge University Press

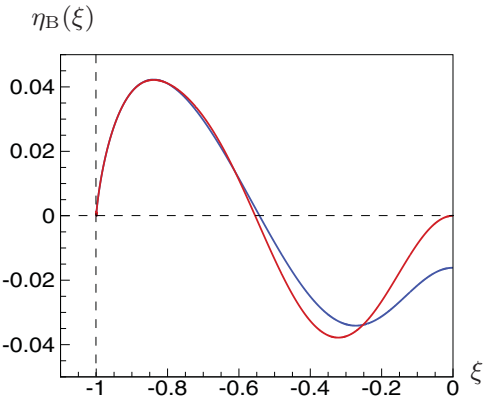

FIGURE 5. The graph of the outer solution for the case $\epsilon = 0.1$, $\kappa = 0.1$, $\lambda_G = 0.8$, $\lambda_0 = 0.4$, $\mathbb{M} = 1.0$, $\hat{\Gamma} = 2$. The top on the left is the graph of the outer solution $\eta_B(\xi)$(with inclusion of the SPE part) over $(-1 < \xi \leqslant 0)$; while the bottom on the right is the graph of the RPE part of outer solution $\epsilon h_1(\xi)$.

$\bar{\mathbb{d}}_0 = -\bar{h}_1(0)$, the full outer solution will be able to satisfy the interface-tip condition: $\eta_B(0,\epsilon) = \bar{\eta}_R(0,\epsilon) + \bar{\eta}_S(0,\epsilon) = 0$ as shown in Figure 5.

However, even including the SPE part, the leading order approximation of the full outer solution still show no interface closure at the bottom of the root, because of the fact, $\lim_{\xi\to-1} \tilde{\mathbb{h}}_0(\xi,\epsilon) = 0$, *decaying exponentially*. It can be shown that the nature of no interface closure remains up to any order approximations of the outer solution. Therefore, the issue of interface closure is determined by some exponentially small quantities beyond all orders, which were missed in the outer solution.

3 Mathematical formulation of problem in the root region

To explore the mechanism of interface closure for steady deep-cellular growth, one must investigate the behaviour of the solution with a different length scale in the root region, $|\xi + 1| \ll 1; |\eta - \eta_B(\xi,\epsilon)| \ll 1$.

Assume that the interface shape function in the root region has the following asymptotic form:

$$\eta_B(\xi,\epsilon) = \delta(\epsilon)\hat{\eta}_B(\hat{\xi},\epsilon); \quad \hat{\eta}_B(\hat{\xi},\epsilon) \sim \left[\hat{\eta}_R(\hat{\xi},\epsilon) + \hat{\eta}_S(\hat{\xi},\epsilon)\right], \tag{3.1}$$

where $\hat{\xi} = (\xi + 1)/\delta(\epsilon)$, $\hat{\eta}_R(\hat{\xi},\epsilon)$ is the RPE part of the inner solution for the interface shape function, $\delta(\epsilon)$ is the asymptotic factor to be determined, so that $|\hat{\eta}_R(\hat{\xi},\epsilon)| = O(1)$; $\hat{\eta}_S(\hat{\xi},\epsilon)$ is the SPE part, it is transcendentally small as $\epsilon \to 0$.

We further assume that the solution for the interface shape function $\eta_B(\xi,\epsilon)$ is analytic at the bottom of the root $\xi = -1$ or $\hat{\xi} = 0$ and satisfies the root smoothness condition. Therefore, one may expand it in the Taylor series: $\eta_B(\xi,\epsilon) = \delta^2\hat{\eta}_b + \bar{\mathbb{o}}_2(1+\xi)^2 + \bar{\mathbb{o}}_3(1+\xi)^3 + \cdots$, subsequently, write the formula: $\hat{\eta}_B(\hat{\xi},\epsilon) \approx \hat{P}_n(\hat{\xi}) = [\hat{\eta}_b + \mathbb{o}_2\hat{\xi}^2 + \mathbb{o}_3\hat{\xi}^3 + \cdots + \mathbb{o}_n\hat{\xi}^n]$, where n is any large integer.

https://doi.org/10.1017/S0956792515000066 Published online by Cambridge University Press

Furthermore, in the far field of root region, from the asymptotic behaviour of RPE part of the outer solution $\bar{h}_1(\xi) \sim \mathbb{o}_0(1+\xi)^\alpha$, as $(\xi \to -1)$, or $\eta_{\rm B}(\xi,\epsilon) \approx \delta(\epsilon)\hat{\eta}_{\rm B}(\hat{\xi},\epsilon) \approx \epsilon\,\mathbb{o}_0(1+\xi)^\alpha = \mathbb{o}_0\epsilon\delta^\alpha(\epsilon)\hat{\xi}^\alpha$, it is deduced that $\delta(\epsilon) = \epsilon\delta^\alpha(\epsilon)$, or, $\delta(\epsilon) = \epsilon^{\frac{1}{1-\alpha}}$ and

$$\hat{\eta}_{\rm B}(\hat{\xi},\epsilon) \approx \mathbb{o}_0\hat{\xi}^\alpha, \quad (\hat{\xi} \gg 1). \tag{3.2}$$

The composite solution of the interface shape in the root region is the function:

$$\hat{\eta}_{\rm T}(\hat{\xi}) \approx \begin{cases} \mathbb{o}_0\hat{\xi}^\alpha, & \text{as} \quad \hat{\xi} \gg 1; \\ \hat{\eta}_{\rm B}(\hat{\xi},\epsilon), & \text{as} \quad \hat{\xi} = O(1). \end{cases} \tag{3.3}$$

In view of the above, in the leading order approximation such a composite solution can be written in the following form:

$$\hat{\eta}_{\rm T}(\hat{\xi}) = \begin{cases} \hat{\eta}_{\rm T}^{(\rm II)}(\hat{\xi}) = \mathbb{o}_0\hat{\xi}^\alpha, & (\rm II): \quad (\hat{\xi}_* < \hat{\xi} < \infty), \\ \hat{\eta}_{\rm T}^{(\rm I)}(\hat{\xi}) = \hat{P}_n(\hat{\xi}), & (\rm I): \quad (0 \leqslant \hat{\xi} < \hat{\xi}_*), \end{cases} \tag{3.4}$$

satisfying the $(n-1)$-th order smoothness conditions:

$$\begin{aligned} &\hat{\eta}_{\rm T}^{(\rm I)}(\hat{\xi}_*) = \hat{\eta}_{\rm T}^{(\rm II)}(\hat{\xi}_*), \\ &\tfrac{{\rm d}^k}{{\rm d}\hat{\xi}^k}\hat{\eta}_{\rm T}^{(\rm I)}(\hat{\xi}_*) = \tfrac{{\rm d}^k}{{\rm d}\hat{\xi}^k}\hat{\eta}_{\rm T}^{(\rm II)}(\hat{\xi}_*), \ (k = 1,2,\ldots,n-1). \end{aligned}$$

As a consequence, we derive that

$$\begin{aligned} &\mathbb{o}_0\hat{\xi}_*^\alpha = \hat{\eta}_* = \hat{\eta}_{\rm b} + \mathbb{o}_2\hat{\xi}_*^2 + \mathbb{o}_3\hat{\xi}_*^3 + \cdots + \mathbb{o}_n\hat{\xi}_*^n \\ &\mathbb{o}_0\alpha\hat{\xi}_*^{\alpha-1} = 2\mathbb{o}_2\hat{\xi}_* + 3\mathbb{o}_3\hat{\xi}_*^2 + \cdots + n\mathbb{o}_n\hat{\xi}_*^{n-1} \\ &\mathbb{o}_0\alpha(\alpha-1)\hat{\xi}_*^{\alpha-2} = 2\mathbb{o}_2 + (3\cdot 2)\mathbb{o}_3\hat{\xi}_* + \cdots + n(n-1)\mathbb{o}_n\hat{\xi}_*^{n-2} \\ &\cdots, \end{aligned}$$

or, in general,

$$\mathbb{o}_0(\alpha-i)!\hat{\xi}_*^{(\alpha-i)} = \sum_{i<m\leqslant n} \mathbb{o}_m\frac{m!\hat{\xi}_*^{m-i}}{(m-i)!}, \quad (i = 1,2,\ldots,n-1). \tag{3.5}$$

The above function $\hat{\eta}_{\rm T}(\hat{\xi})$ has up to $(n-1)$-th order continuous derivatives in the entire root region $(0 \leqslant \hat{\xi} < \infty)$. With the n conditions (3.5), the n coefficients of $\hat{P}_n(\hat{\xi})$: $\{\hat{\eta}_{\rm b}, \mathbb{o}_2, \ldots, \mathbb{o}_n\}$ are fully determined as the functions of joint point $\hat{\xi}_*$. In the leading order approximation, we shall set $\hat{\eta}_{\rm R}(\hat{\xi},\epsilon) \approx \hat{P}_3(\hat{\xi})$, accordingly, the corresponding composite solution is described as

$$\hat{\eta}_{\rm T}(\hat{\xi}) = \begin{cases} \mathbb{o}_0\hat{\xi}^\alpha, & (\rm II): \quad (\hat{\xi}_* < \hat{\xi} < \infty), \\ \hat{\eta}_{\rm b} + \mathbb{o}_2\hat{\xi}^2 + \mathbb{o}_3\hat{\xi}^3, & (\rm I): \quad (0 \leqslant \hat{\xi} < \hat{\xi}_*), \end{cases} \tag{3.6}$$

as sketched in Figure 6. In this case $(n = 3)$, the function $\hat{\eta}_{\rm T}(\hat{\xi})$ has continuous up to second order derivatives in the entire root region $(0 \leqslant \hat{\xi} < \infty)$, and the coefficients $\hat{\eta}_*$, $\hat{\eta}_{\rm b}$,

https://doi.org/10.1017/S0956792515000066 Published online by Cambridge University Press

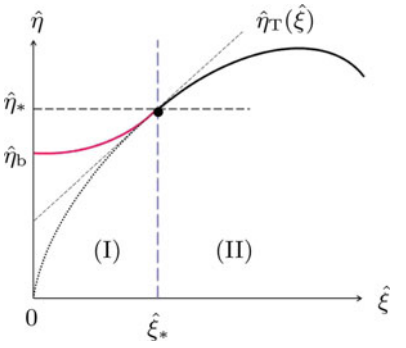

FIGURE 6. The sketch of the function $\hat{\eta}_{\mathrm{T}}(\hat{\xi})$ in the root region.

$\mathbb{O}_2$ and $\mathbb{O}_3$ are derived as the following functions of $\hat{\xi}_*$:

$$\hat{\eta}_* = \mathbb{O}_0 \hat{\xi}_*^{\alpha}, \quad \hat{\eta}_{\mathrm{b}} = \left[1 - \tfrac{\alpha(5-\alpha)}{6}\right] \hat{\eta}_*$$
$$\mathbb{O}_2 = \tfrac{\alpha(3-\alpha)\hat{\eta}_*}{2\hat{\xi}_*^2} \quad \mathbb{O}_3 = -\tfrac{\alpha(2-\alpha)\hat{\eta}_*}{3\hat{\xi}_*^3}.$$

It will be seen later that the parameter $\hat{\xi}_*$ can be determined as the eigenvalue of an EVP.

We now define the root variables $\hat{\xi}$ and $\hat{\eta}$ in the root region as

$$\hat{\xi} = \frac{1+\xi}{\delta(\epsilon)}, \quad \hat{\eta} = \frac{\eta - \delta(\epsilon)\hat{\eta}_{\mathrm{T}}(\hat{\xi})}{\delta(\epsilon)} = \frac{\eta}{\delta(\epsilon)} - \hat{\eta}_{\mathrm{T}}(\hat{\xi}). \tag{3.7}$$

From (3.7), we derive that

$$\begin{aligned}
&\tfrac{\partial}{\partial \eta} = \tfrac{1}{\delta(\epsilon)} \tfrac{\partial}{\partial \hat{\eta}}, \quad \tfrac{\partial^2}{\partial \eta} = \tfrac{1}{\delta^2(\epsilon)} \tfrac{\partial^2}{\partial \hat{\eta}^2}, \\
&\tfrac{\partial}{\partial \xi} = \tfrac{1}{\delta(\epsilon)} \left[\tfrac{\partial}{\partial \hat{\xi}} - \hat{\eta}_{\mathrm{T}}'(\hat{\xi}) \tfrac{\partial}{\partial \hat{\eta}}\right], \\
&\tfrac{\partial^2}{\partial \xi^2} = \tfrac{1}{\delta^2(\epsilon)} \left[\tfrac{\partial^2}{\partial \hat{\xi}^2} + \hat{\eta}_{\mathrm{T}}'^2(\hat{\xi}) \tfrac{\partial^2}{\partial \hat{\eta}^2} - 2\hat{\eta}_{\mathrm{T}}'(\hat{\xi}) \tfrac{\partial^2}{\partial \hat{\eta} \partial \hat{\xi}} - \hat{\eta}_{\mathrm{T}}''(\hat{\xi}) \tfrac{\partial}{\partial \hat{\eta}}\right],
\end{aligned} \tag{3.8}$$

The concentration field in the inner region can be considered as the function of the inner variables $\{\hat{\xi}, \hat{\eta}\}$, namely,

$$C_{\mathrm{B}}(\xi, \eta, \epsilon) = C_{\mathrm{B}}\left[-1 + \delta(\epsilon)\hat{\xi},\, \delta(\epsilon)(\hat{\eta} + \hat{\eta}_{\mathrm{T}}), \epsilon\delta(\epsilon)(\hat{\eta} + \hat{\eta}_{\mathrm{T}})\right] = \hat{C}_{\mathrm{B}}(\hat{\xi}, \hat{\eta}, \epsilon). \tag{3.9}$$

We write the inner solution in the following form:

$$\begin{aligned}
\hat{C}_{\mathrm{B}}(\hat{\xi}, \hat{\eta}, \epsilon) &= \hat{C}_{\mathrm{R}}(\hat{\xi}, \hat{\eta}, \epsilon) + \hat{C}_{\mathrm{S}}(\hat{\xi}, \hat{\eta}, \epsilon), \\
\hat{\eta}_{\mathrm{B}}(\xi, \epsilon) &= \hat{\eta}_{\mathrm{R}}(\hat{\xi}, \epsilon) + \hat{\eta}_{\mathrm{S}}(\hat{\xi}, \epsilon),
\end{aligned} \tag{3.10}$$

where $\hat{C}_{\mathrm{R}}(\hat{\xi}, \hat{\eta}, \epsilon)$ with $\hat{\eta}_{\mathrm{R}}(\hat{\xi}, \epsilon) = 0$ is the RPE-part of the inner solution, while $\hat{C}_{\mathrm{S}}(\hat{\xi}, \hat{\eta}, \epsilon)$ with $\hat{\eta}_{\mathrm{S}}(\hat{\xi}, \epsilon)$ is the SPE-part of the inner solution. In the leading order approximation, we

https://doi.org/10.1017/S0956792515000066 Published online by Cambridge University Press

find

$$\hat{C}_{\mathrm{R}}(\hat{\xi},\hat{\eta},\epsilon) \Longleftrightarrow \bar{C}_{\mathrm{R}}(\xi,\eta,\epsilon) \approx y_{*0} - \epsilon \ln \delta(\epsilon) W \lambda_G \hat{Y}_* + \epsilon \left[y_{*1} - W \lambda_G \hat{Y}_0(\hat{\xi},\hat{\eta}) \right]. \quad (3.11)$$

The major task for us is to find the second, SPE-part of root solution $\{\hat{C}_{\mathrm{S}}(\hat{\xi},\hat{\eta},\epsilon),\hat{\eta}_{\mathrm{S}}(\hat{\xi},\epsilon)\}$, which is transcendentally small as $\epsilon \to 0$.

4 The singular perturbation expansion part of inner solution in the root region

The inner systems governing the SPE-part of solution $\{\hat{C}_{\mathrm{S}}(\hat{\xi},\hat{\eta},\epsilon),\hat{\eta}_{\mathrm{S}}(\hat{\xi},\epsilon)\}$ can be obtained from (2.2)–(2.4). In doing so, one needs to change the outer variables (ξ,η) to the inner variables $(\hat{\xi},\hat{\eta})$ and expand all the coordinate functions into the asymptotic forms, as $\epsilon \to 0$ with fixed $(\hat{\xi},\hat{\eta})$. For convenience of the readers, we list the results below [14–16]:

$$\begin{aligned}
&\mathscr{R}(\xi,\eta) = \pi^2\delta^2(\epsilon)(\hat{\eta}+\hat{\eta}_{\mathrm{T}})^2 + \pi^2\delta^2(\epsilon)\hat{\xi}^2 + \cdots,\\
&\Theta(\xi,\eta) = -\arctan\left(\tfrac{\hat{\xi}}{\hat{\eta}+\hat{\eta}_{\mathrm{T}}}\right) + \cdots;
\end{aligned}$$

$$\begin{aligned}
&\hat{X}(\hat{\xi},\hat{\eta},\epsilon) \sim -1 + \tfrac{2(1-\lambda_0)}{\pi}\arctan\left(\tfrac{\hat{\xi}}{\hat{\eta}+\hat{\eta}_{\mathrm{T}}}\right) + \cdots\\
&\hat{Y}(\hat{\xi},\hat{\eta},\epsilon) \sim \ln\delta(\epsilon)\hat{Y}_* + \hat{Y}_0(\hat{\xi},\hat{\eta}) + \delta(\epsilon)\hat{Y}_1(\hat{\xi},\hat{\eta}) + \cdots,\\
&Y_\eta(\xi,\eta) \;= \tfrac{1}{\delta(\epsilon)}\hat{Y}_{\hat{\eta}}(\hat{\xi},\hat{\eta},\epsilon) \sim \tfrac{1}{\delta(\epsilon)}\hat{Y}_{\hat{\eta},0}(\hat{\xi},\hat{\eta}) + \hat{Y}_{\hat{\eta},1}(\hat{\xi},\hat{\eta}) + \cdots,\\
&Y_\xi(\xi,\eta) \;= \tfrac{1}{\delta(\epsilon)}\hat{Y}_{\hat{\xi}}(\hat{\xi},\hat{\eta},\epsilon) \sim \tfrac{1}{\delta(\epsilon)}\hat{Y}_{\hat{\xi},0}(\hat{\xi},\hat{\eta}) + \cdots,
\end{aligned} \quad (4.1)$$

where

$$\begin{aligned}
&\hat{Y}_* = \frac{2(1-\lambda_0)}{\pi}, \quad \hat{Y}_0 = \frac{(1-\lambda_0)}{\pi}\ln\frac{\pi^2\left[(\hat{\eta}+\hat{\eta}_{\mathrm{T}})^2+\hat{\xi}^2\right]}{4}, \quad \hat{Y}_1 = \lambda_0(\hat{\eta}+\hat{\eta}_{\mathrm{T}}),\\
&\hat{Y}_{\hat{\eta},0}(\hat{\xi},\hat{\eta}) = \frac{2(1-\lambda_0)}{\pi}\frac{(\hat{\eta}+\hat{\eta}_{\mathrm{T}})}{\hat{\xi}^2+(\hat{\eta}+\hat{\eta}_{\mathrm{T}})^2}, \quad \hat{Y}_{\hat{\eta},1}(\hat{\xi},\hat{\eta}) = \lambda_0,\\
&\hat{Y}_{\hat{\xi},0}(\hat{\xi},\hat{\eta}) = \frac{2(1-\lambda_0)}{\pi}\frac{\hat{\xi}}{\hat{\xi}^2+(\hat{\eta}+\hat{\eta}_{\mathrm{T}})^2},
\end{aligned} \quad (4.2)$$

and

$$\begin{aligned}
&\mathscr{G}(\xi,\eta) = \sqrt{Y_\xi^2+Y_\eta^2} = \frac{1}{\delta(\epsilon)}\hat{\mathscr{G}}(\hat{\xi},\hat{\eta},\epsilon) \sim \frac{1}{\delta(\epsilon)}\hat{\mathscr{G}}_0(\hat{\xi},\hat{\eta}) + \cdots,\\
&\hat{\mathscr{G}}_0(\hat{\xi},\hat{\eta}) = \frac{2(1-\lambda_0)}{\pi}\frac{1}{\sqrt{\hat{\xi}^2+(\hat{\eta}+\hat{\eta}_{\mathrm{T}})^2}}.
\end{aligned} \quad (4.3)$$

https://doi.org/10.1017/S0956792515000066 Published online by Cambridge University Press

Moreover, one may write

$$\begin{aligned}\mathscr{K}\{\delta(\epsilon)\hat{\eta}_{\mathrm{B}}\} &= -\frac{1}{\hat{\mathscr{G}}_0(\hat{\xi},0)}\frac{\partial^2\hat{\eta}_{\mathrm{B}}}{\partial\hat{\xi}^2} + \hat{\mathscr{K}}_0(\hat{\xi},0) + O\big(\hat{\eta}_{\mathrm{B}}\big),\\ \hat{\mathscr{K}}_0(\hat{\xi},0) &= -\frac{\pi}{2(1-\lambda_0)}\frac{\hat{\eta}_{\mathrm{T}}}{\sqrt{\hat{\xi}^2+\hat{\eta}_{\mathrm{T}}^2}}.\end{aligned} \tag{4.4}$$

By showing only the lowest order small terms, one may write the inner equation as

$$\frac{\partial^2\hat{C}_{\mathrm{S}}}{\partial\hat{\xi}^2} + \Big[1+\hat{\eta}_{\mathrm{T}}'^2(\hat{\xi})\Big]\frac{\partial^2\hat{C}_{\mathrm{S}}}{\partial\hat{\eta}^2} - 2\hat{\eta}_{\mathrm{T}}'(\hat{\xi})\frac{\partial^2\hat{C}_{\mathrm{S}}}{\partial\hat{\eta}\partial\hat{\xi}} = O(\text{h.o.t.}). \tag{4.5}$$

The interface conditions in the root region can be linearized along $\hat{\eta}=0$ and it follows that at $\hat{\eta}=0$,

$$\hat{C}_{\mathrm{S}} + \frac{\partial\hat{C}_{\mathrm{R}}}{\partial\hat{\eta}}\hat{\eta}_{\mathrm{S}} = -\epsilon W\lambda_G\frac{\partial\hat{Y}_0}{\partial\hat{\eta}}\hat{\eta}_{\mathrm{S}} + \frac{\epsilon^2\hat{\Gamma}}{\mathbb{M}W\hat{\mathscr{G}}_0(\hat{\xi},0)}\frac{\partial^2\hat{\eta}_{\mathrm{S}}}{\partial\hat{\xi}^2} + O(\text{h.o.t.}), \tag{4.6}$$

and

$$\begin{aligned}&\frac{\partial\hat{C}_{\mathrm{S}}}{\partial\hat{\eta}} + \frac{\partial^2\hat{C}_{\mathrm{R}}}{\partial\hat{\eta}^2}\hat{\eta}_{\mathrm{S}} - \frac{\partial\hat{\eta}_{\mathrm{S}}}{\partial\hat{\xi}}\frac{\partial\hat{C}_{\mathrm{R}}}{\partial\hat{\xi}} - \epsilon W(1-\kappa)\hat{C}_{\mathrm{R}}\hat{Y}_{\hat{\xi},0}\frac{\partial\hat{\eta}_{\mathrm{S}}}{\partial\hat{\xi}}\\ &\quad + \epsilon W(1-\kappa)\hat{C}_{\mathrm{S}}\hat{Y}_{\hat{\eta},0} + \epsilon W(1-\kappa)\hat{Y}_{\hat{\eta},0}\frac{\partial\hat{C}_{\mathrm{R}}}{\partial\hat{\eta}}\hat{\eta}_{\mathrm{S}}\\ &\quad + \epsilon W(1-\kappa)\hat{C}_{\mathrm{R}}\hat{Y}_{\hat{\eta}\hat{\eta},0}\hat{\eta}_{\mathrm{S}} = O(\text{h.o.t.}).\end{aligned} \tag{4.7}$$

The system (4.5)–(4.7) is a linear homogeneous system of PDE's, which can be solved by using the multiple variables expansion method. Presuming that the SPE-part of root solutions contains the multiple length scales, we introduce the following fast root variables:

$$\begin{cases}\hat{\xi}_+ = \dfrac{\hat{\phi}(\hat{\xi},\hat{\eta})}{\hat{\beta}(\epsilon)} = \dfrac{1}{\hat{\beta}(\epsilon)}\displaystyle\int_0^{\hat{\xi}}\hat{k}(\hat{\xi}_1,\hat{\eta})\mathrm{d}\hat{\xi}_1,\\ \hat{\eta}_+ = \dfrac{\hat{\psi}(\hat{\xi},\hat{\eta})}{\hat{\beta}(\epsilon)} = \dfrac{1}{\hat{\beta}(\epsilon)}\displaystyle\int_0^{\hat{\eta}}\frac{\hat{k}(\hat{\xi},\hat{\eta}_1)}{\sqrt{1+\hat{\eta}_{\mathrm{T}}'^2}}\mathrm{d}\hat{\eta}_1,\end{cases} \tag{4.8}$$

where $\hat{\beta}$ is to be determined. In the above, we have assumed that

$$\hat{\phi}_{\hat{\xi}} = \sqrt{1+\hat{\eta}_{\mathrm{T}}'^2}\,\hat{\psi}_{\hat{\eta}} = \hat{k}(\hat{\xi},\hat{\eta}). \tag{4.9}$$

Furthermore, we write

$$\hat{\psi}_{\hat{\xi}} = -\sqrt{1+\hat{\eta}_{\mathrm{T}}'^2}\,\hat{\phi}_{\hat{\eta}} = \hat{g}(\hat{\xi},\hat{\eta}). \tag{4.10}$$

In terms of these multiple variables $(\hat{\xi},\hat{\eta},\hat{\xi}_+,\hat{\eta}_+)$, we express the SPE part of the root solution as

$$\hat{C}_{\mathrm{S}}(\hat{\xi},\hat{\eta},\epsilon) = \hat{\mathbb{C}}_*(\hat{\xi},\hat{\eta},\hat{\xi}_+,\hat{\eta}_+,\epsilon),\quad \hat{\eta}_{\mathrm{S}}(\hat{\xi},\epsilon) = \hat{\mathbb{h}}_*(\hat{\xi},\hat{\xi}_+,\epsilon),$$

https://doi.org/10.1017/S0956792515000066 Published online by Cambridge University Press

where $(\hat{\xi}, \hat{\eta}, \hat{\xi}_+, \hat{\eta}_+)$ are formally treated as the independent variables. Then the inner system (4.5)–(4.7) can be converted into the form with the multiple variables $(\hat{\xi}, \hat{\eta}, \hat{\xi}_+, \hat{\eta}_+)$. We only consider the leading order approximation in the limit of $\epsilon \to 0$:

$$\begin{aligned}
\hat{\mathbb{C}}_*(\hat{\xi}, \hat{\eta}, \hat{\xi}_+, \hat{\eta}_+, \epsilon) &\sim \epsilon \hat{b}_{*0}(\epsilon) \hat{\mathbb{C}}_{*0}(\hat{\xi}, \hat{\eta}, \hat{\xi}_+, \hat{\eta}_+), \\
\hat{\mathbb{h}}_s(\hat{\xi}, \hat{\xi}_+, \epsilon) &\sim \hat{b}_{*0}(\epsilon) \hat{\mathbb{h}}_{*0}(\hat{\xi}, \hat{\xi}_+), \\
\hat{k}(\hat{\xi}, \hat{\eta}, \epsilon) &\sim \hat{k}_0(\hat{\xi}, \hat{\eta}), \\
\hat{g}(\hat{\xi}, \hat{\eta}, \epsilon) &\sim \hat{g}_0(\hat{\xi}, \hat{\eta}),
\end{aligned} \tag{4.11}$$

where $|\hat{b}_{*0}(\epsilon)| \ll 1$ is an asymptotic factor.

4.1 The zeroth order approximation $O(1)$

By balancing both sides of the interface conditions (4.5)–(4.7), we derive that

$$\hat{\beta} = \sqrt{\epsilon \hat{\Gamma}}, \tag{4.12}$$

and leading order equation as

$$(\hat{k}_0^2 + \hat{g}_0^2) \left(\frac{\partial^2 \hat{C}_{*0}}{\partial \hat{\xi}_+^2} + \frac{\partial^2 \hat{C}_{*0}}{\partial \hat{\eta}_+^2} \right) + 2\hat{\eta}_{\mathrm{T}}' \left[\frac{\hat{k}_0 \hat{g}_0}{\mathbb{G}_{\mathrm{T}}} \left(\frac{\partial^2 \hat{C}_{*0}}{\partial \hat{\xi}_+^2} - \frac{\partial^2 \hat{C}_{*0}}{\partial \hat{\eta}_+^2} \right) - \frac{\hat{k}_0^2 - \hat{g}_0^2}{\mathbb{G}_{\mathrm{T}}} \frac{\partial^2 \hat{C}_{*0}}{\partial \hat{\xi}_+ \partial \hat{\eta}_+} \right] = 0. \tag{4.13}$$

We now set $\hat{g}_0(\hat{\xi}, \hat{\eta}) = \hat{k}_0(\hat{\xi}, \hat{\eta})$. It follows from (4.9)–(4.10) that $\hat{k}_0 = \int_0^{\hat{\eta}} \frac{\partial}{\partial \hat{\xi}} \left[\hat{k}_0 / (1 + \hat{\eta}_{\mathrm{T}}'^2)^{1/2} \right] \mathrm{d}\hat{\eta}$, so that

$$\frac{\partial \hat{k}_0}{\partial \hat{\eta}} - \frac{\partial}{\partial \hat{\xi}} \left[\frac{\hat{k}_0}{\sqrt{1 + \hat{\eta}_{\mathrm{T}}'^2}} \right] = 0. \tag{4.14}$$

This is a governing equation of $\hat{k}_0(\hat{\xi}, \hat{\eta})$, and can be solved for the function $\hat{k}_0(\hat{\xi}, \hat{\eta})$, provided the boundary value $\hat{k}_0(\hat{\xi}) = \hat{k}_0(\hat{\xi}, 0)$ is determined. Furthermore, in this case, (4.13) reduces to

$$\left(1 + \frac{\hat{\eta}_{\mathrm{T}}'}{\mathbb{G}_{\mathrm{T}}} \right) \frac{\partial^2 \hat{C}_{*0}}{\partial \hat{\xi}_+^2} + \left(1 - \frac{\hat{\eta}_{\mathrm{T}}'}{\mathbb{G}_{\mathrm{T}}} \right) \frac{\partial^2 \hat{C}_{*0}}{\partial \hat{\eta}_+^2} = 0. \tag{4.15}$$

In [11], the authors had mistakenly over-simplified (4.15) to Laplace's equation:

$$\frac{\partial^2 \hat{\mathbb{C}}_{*0}}{\partial \hat{\xi}_+^2} + \frac{\partial^2 \hat{\mathbb{C}}_{*0}}{\partial \hat{\eta}_+^2} = 0. \tag{4.16}$$

However, this equation missed the crucial terms containing the $\hat{\eta}_{\mathrm{T}}'/\mathbb{G}_{\mathrm{T}} = O(1)$ in (4.15), which describe the curviness of the interface in the root region. The role of these missed terms is critical for generating the mechanism of interface closure. It is the presence of these terms that results in the turning point singularity and determines the multiple-layer structure of the inner solution.

https://doi.org/10.1017/S0956792515000066 Published online by Cambridge University Press

The interface conditions in leading order approximation are: at the interface $\hat{\eta} = \hat{\eta}_+ = 0$,

$$\hat{C}_{*0} = \frac{\hat{k}_0^2}{\mathbb{M}W\hat{\mathscr{G}}_0(\hat{\xi},0)}\frac{\partial^2\hat{\mathbb{h}}_{*0}}{\partial\hat{\xi}_+^2}, \tag{4.17}$$

$$\frac{\hat{k}_0}{\sqrt{1+\hat{\eta}_{\mathrm{T}}'^2}}\left(\frac{\partial\hat{C}_{*0}}{\partial\hat{\eta}_+}-\frac{\partial\hat{C}_{*0}}{\partial\hat{\xi}_+}\right)-\hat{k}_0W\left[(1-\kappa)y_{*0}-\lambda_{\mathrm{G}}\right]\hat{Y}_{\hat{\xi},0}(\hat{\xi},0)\frac{\partial\hat{\mathbb{h}}_{*0}}{\partial\hat{\xi}_+}=0. \tag{4.18}$$

The system allows the following normal modes solutions:

$$\begin{aligned}\hat{C}_{*0} &= \tilde{A}_{*0}(\hat{\xi},\hat{\eta})\exp\left\{\mathrm{i}\hat{\xi}_+-\lambda_c\hat{\eta}_+\right\},\\ \hat{\mathbb{h}}_{*0} &= \tilde{D}_{*0}\exp\left\{\mathrm{i}\hat{\xi}_+\right\},\end{aligned} \tag{4.19}$$

where the coefficient $\tilde{D}_{*0}$ is a free constant and $\lambda_c = [(\mathbb{G}_{\mathrm{T}}+\hat{\eta}_{\mathrm{T}}')/(\mathbb{G}_{\mathrm{T}}-\hat{\eta}_{\mathrm{T}}')]^{1/2}$. From (4.17), we derive

$$\hat{A}_{*0}(\hat{\xi}) = \tilde{A}_{*0}(\hat{\xi},0) = -\tilde{D}_{*0}\frac{\hat{k}_0^2}{\mathbb{M}W\hat{\mathscr{G}}_0(\hat{\xi},0)}.$$

From (4.18), we derive

$$-\frac{\hat{A}_{*0}(\hat{\xi})}{\sqrt{1+\hat{\eta}_{\mathrm{T}}'^2}}\hat{k}_0(\lambda_c+\mathrm{i})-\mathrm{i}\hat{k}_0W\left[(1-\kappa)y_{*0}-\lambda_{\mathrm{G}}\right]\hat{Y}_{\hat{\xi},0}(\hat{\xi},0)\tilde{D}_{*0}=0,$$

or

$$\frac{\hat{A}_{*0}(\hat{\xi})}{\sqrt{1+\hat{\eta}_{\mathrm{T}}'^2}}\hat{k}_0(\lambda_c+\mathrm{i})+\mathrm{i}\hat{k}_0W\left[(1-\kappa)y_{*0}-\lambda_{\mathrm{G}}\right]\hat{Y}_{\hat{\xi},0}(\hat{\xi},0)\tilde{D}_{*0}=0.$$

In order to satisfy the interface conditions (4.17) and (4.18) the function $\hat{k}_0(\hat{\xi})$ must be subject to the formula:

$$-\frac{(\lambda_c+\mathrm{i})\hat{k}_0^3}{\mathbb{M}W\hat{\mathscr{G}}_0(\hat{\xi},0)\sqrt{1+\hat{\eta}_{\mathrm{T}}'^2}}+\mathrm{i}\hat{k}_0W\hat{Y}_{\hat{\xi},0}(\hat{\xi},0)\left[(1-\kappa)y_{*0}-\lambda_{\mathrm{G}}\right]=0. \tag{4.20}$$

There are three roots for $\hat{k}_0$:

$$\begin{cases}\hat{k}_0^{(1)}(\hat{\xi}) = \hat{k}_s(\hat{\xi}) = \left(\dfrac{\mathrm{i}}{\lambda_c+\mathrm{i}}\right)^{\frac{1}{2}}\hat{\mathbb{m}}\sqrt{\hat{\mathscr{G}}_0(\hat{\xi},0)\hat{Y}_{\hat{\xi},0}(\hat{\xi},0)}\left(1+\hat{\eta}_{\mathrm{T}}'^2\right)^{\frac{1}{4}}\\ \hat{k}_0^{(2)}(\hat{\xi}) = -\hat{k}_s(\hat{\xi}) = -\left(\dfrac{\mathrm{i}}{\lambda_c+\mathrm{i}}\right)^{\frac{1}{2}}\hat{\mathbb{m}}\sqrt{\hat{\mathscr{G}}_0(\hat{\xi},0)\hat{Y}_{\hat{\xi},0}(\hat{\xi},0)}\left(1+\hat{\eta}_{\mathrm{T}}'^2\right)^{\frac{1}{4}}\\ \hat{k}_0^{(3)}(\hat{\xi}) = 0,\end{cases} \tag{4.21}$$

where we have defined

$$\hat{\mathbb{m}} = W\sqrt{\mathbb{M}\left[(1-\kappa)y_{*0}-\lambda_{\mathrm{G}}\right]}. \tag{4.22}$$

https://doi.org/10.1017/S0956792515000066 Published online by Cambridge University Press

Recalling the formulas

$$\begin{cases} \hat{\mathscr{G}}_0(\hat{\xi},0) &= \frac{2(1-\lambda_0)}{\pi}\frac{1}{\sqrt{\hat{\xi}^2+\hat{\eta}_{\mathrm{T}}^2(\hat{\xi})}} \\ \hat{Y}_{\hat{\xi},0}(\hat{\xi},0) &= \frac{2(1-\lambda_0)}{\pi}\frac{\hat{\xi}}{\hat{\xi}^2+\hat{\eta}_{\mathrm{T}}^2(\hat{\xi})} > 0, \quad (0 \leqslant \hat{\xi} < \infty), \end{cases} \tag{4.23}$$

one may re-write

$$\hat{k}_s(\hat{\xi}) = \left(\frac{\mathrm{i}}{\lambda_c+\mathrm{i}}\right)^{\frac{1}{2}} \frac{2(1-\lambda_0)\mathrm{i}\hat{m}}{\pi} \frac{\hat{\xi}^{\frac{1}{2}}}{\left[\hat{\xi}^2+\hat{\eta}_{\mathrm{T}}^2(\hat{\xi})\right]^{\frac{3}{4}}}\left(1+\hat{\eta}_{\mathrm{T}}'^2\right)^{\frac{1}{4}}. \tag{4.24}$$

In accordance with the above, we obtain three fundamental solutions:

$$\begin{aligned} \hat{H}_1(\hat{\xi}) &= \mathrm{e}^{\frac{\mathrm{i}}{\sqrt{\epsilon\hat{\Gamma}}}\hat{\chi}(\hat{\xi})} = \mathrm{e}^{-\frac{\hat{\chi}_{\mathrm{I}}(\hat{\xi})}{\sqrt{\epsilon\hat{\Gamma}}}}\left[\cos\left(\frac{\hat{\chi}_{\mathrm{R}}(\hat{\xi})}{\sqrt{\epsilon\hat{\Gamma}}}\right)+\mathrm{i}\sin\left(\frac{\hat{\chi}_{\mathrm{R}}(\hat{\xi})}{\sqrt{\epsilon\hat{\Gamma}}}\right)\right], \\ \hat{H}_2(\hat{\xi}) &= \mathrm{e}^{-\frac{\mathrm{i}}{\sqrt{\epsilon\hat{\Gamma}}}\hat{\chi}(\hat{\xi})} = \mathrm{e}^{\frac{\hat{\chi}_{\mathrm{I}}(\hat{\xi})}{\sqrt{\epsilon\hat{\Gamma}}}}\left[\cos\left(\frac{\hat{\chi}_{\mathrm{R}}(\hat{\xi})}{\sqrt{\epsilon\hat{\Gamma}}}\right)-\mathrm{i}\sin\left(\frac{\hat{\chi}_{\mathrm{R}}(\hat{\xi})}{\sqrt{\epsilon\hat{\Gamma}}}\right)\right], \\ \hat{H}_3(\hat{\xi}) &= 1, \end{aligned} \tag{4.25}$$

where we have defined

$$\begin{aligned} \hat{\chi}(\hat{\xi}) &= \int_a^{\hat{\xi}} \hat{k}_s(\hat{\xi}_1)\mathrm{d}\hat{\xi}_1 = \hat{\chi}_{\mathrm{R}}(\hat{\xi})+\mathrm{i}\hat{\chi}_{\mathrm{I}}(\hat{\xi}) \\ &= \frac{2(1-\lambda_0)\mathrm{i}\hat{m}}{\pi}\int_a^{\hat{\xi}}\left[\frac{\mathrm{i}}{\lambda_c(\hat{\xi}_1)+\mathrm{i}}\right]^{\frac{1}{2}}\frac{\hat{\xi}_1^{\frac{1}{2}}(1+\hat{\eta}_{\mathrm{T}}'^2)^{\frac{1}{4}}}{[\hat{\xi}_1^2+\hat{\eta}_{\mathrm{T}}^2(\hat{\xi}_1)]^{\frac{3}{4}}}\mathrm{d}\hat{\xi}_1. \end{aligned} \tag{4.26}$$

Here, the lower limit a can be chosen arbitrarily. The fundamental solutions $\hat{H}_1(\hat{\xi}), \hat{H}_2(\hat{\xi}), \hat{H}_3(\hat{\xi})$ can be called the H-waves. One may write the general inner solution in the root region as

$$\hat{\mathbb{h}}_{*0}(\hat{\xi},\hat{\xi}_+) = \tilde{d}_1\hat{H}_1(\hat{\xi})+\tilde{d}_2\hat{H}_2(\hat{\xi})+\tilde{d}_3\hat{H}_3(\hat{\xi}), \tag{4.27}$$

where $(\tilde{d}_1,\tilde{d}_2,\tilde{d}_3)$ are arbitrary constants. To match with the outer solution, the constant solution $\hat{H}_3(\hat{\xi})$ for the interface shape function should be ruled out. Hence, one may write the general solution in the root inner region as

$$\hat{\mathbb{h}}_{*0}(\hat{\xi},\hat{\xi}_+) = \tilde{d}_1\hat{H}_1(\hat{\xi})+\tilde{d}_2\hat{H}_2(\hat{\xi}). \tag{4.28}$$

The pair of coefficients $(\tilde{d}_1,\tilde{d}_2)$ may have different values in different sub-regions which will be determined in following sections.

4.2 The root inner solution in the sub-region (II)

The sub-region (II) contains the far field of the root region $\hat{\xi} \gg 1$, where the solution must match with the outer solution. It may be deduced that the root solution only contains one wave type basic solution $\hat{H}_2(\hat{\xi})$ in sub-region (II). As a matter of the fact, in order to

https://doi.org/10.1017/S0956792515000066 Published online by Cambridge University Press

match with the outer solution,

$$\eta_{\mathrm{B}}(\xi,\epsilon)=\epsilon\left[\bar{h}_1(\xi)+\bar{\mathbb{h}}_0(\xi,\epsilon)+\cdots\right], \tag{4.29}$$

where

$$\bar{\mathbb{h}}_0(\xi,\epsilon)=-\Re\{\bar{h}_1(0)H_2(\xi)\}=-\bar{h}_1(0)\mathrm{e}^{\frac{\chi_1(\xi)}{\sqrt{\epsilon\hat{\Gamma}}}}\cos\left(\frac{\chi_{\mathrm{R}}(\xi)}{\sqrt{\epsilon\hat{\Gamma}}}\right)\to 0$$

exponentially decays as $\xi\to-1$, the inner solutions of the interface shape function must have the form:

$$\hat{\eta}_{\mathrm{B}}(\hat{\xi},\epsilon)=\delta(\epsilon)\left[\hat{\eta}_{\mathrm{T}}(\hat{\xi})+\hat{b}_{*0}(\epsilon)\hat{d}_2\hat{H}_2(\hat{\xi})+\cdots\right], \tag{4.30}$$

where $\hat{H}_2(\hat{\xi})$ increases exponentially as $\hat{\xi}\to\infty$. The first terms on the right-hand side of (4.29) and (4.30) are obviously matched. To match the SPE part of the inner solution, $\hat{b}_{*0}(\epsilon)\hat{\mathbb{h}}_{*0}(\hat{\xi},\hat{\xi}_+)=\hat{b}_{*0}(\epsilon)\hat{d}_2\hat{H}_2(\hat{\xi})$ with the SPE part of the outer solution, $\epsilon\bar{\mathbb{h}}_0(\xi,\epsilon)$, we write $\hat{\xi}_0=\frac{1}{\delta(\epsilon)}$. Obviously, the point $\hat{\xi}=\hat{\xi}_0$ as the inner variable corresponds to the point $\xi=0$ as the outer variable. By choosing the lower limit $a=0$, it follows from (4.26) that

$$\hat{\chi}(\hat{\xi}_0)=\mathrm{e}^{\frac{\mathrm{i}\pi}{4}}\frac{2(1-\lambda_0)\mathbb{m}\hat{\mathbb{m}}}{\pi}\int_0^{\hat{\xi}_0}\frac{\hat{\xi}_1^{\frac{1}{2}}\left[1+\hat{\eta}_{\mathrm{T}}'^2(\hat{\xi}_1)\right]^{\frac{1}{4}}}{[\hat{\xi}_1^2+\hat{\eta}_{\mathrm{T}}^2(\hat{\xi}_1)]^{\frac{3}{4}}}\mathrm{d}\hat{\xi}_1, \tag{4.31}$$

and

$$\hat{\chi}(\hat{\xi})=\mathrm{e}^{\frac{\mathrm{i}\pi}{4}}\frac{2(1-\lambda_0)\mathbb{m}\hat{\mathbb{m}}}{\pi}\left[\int_0^{\hat{\xi}_0}\frac{\hat{\xi}_1^{\frac{1}{2}}\left[1+\hat{\eta}_{\mathrm{T}}'^2(\hat{\xi}_1)\right]^{\frac{1}{4}}}{[\hat{\xi}_1^2+\hat{\eta}_{\mathrm{T}}^2(\hat{\xi}_1)]^{\frac{3}{4}}}\mathrm{d}\hat{\xi}_1+\int_{\hat{\xi}_0}^{\hat{\xi}}\frac{\hat{\xi}_1^{\frac{1}{2}}\left[1+\hat{\eta}_{\mathrm{T}}'^2(\hat{\xi}_1)\right]^{\frac{1}{4}}}{[\hat{\xi}_1^2+\hat{\eta}_{\mathrm{T}}^2(\hat{\xi}_1)]^{\frac{3}{4}}}\mathrm{d}\hat{\xi}_1\right]. \tag{4.32}$$

On the other hand, as

$$\chi(\xi)=\int_0^{\xi}W\sqrt{\mathbb{M}\Delta_0\mathscr{G}_0(\xi_1,0)}\left[1+\frac{\mathrm{i}}{\lambda_0}Y_{\xi,0}(\xi_1,0)\right]^{\frac{1}{2}}\mathrm{d}\xi_1, \tag{4.33}$$

and with the inner variable, the interval $(0,\xi)$ is changed to interval $(\hat{\xi}_0,\hat{\xi})$, we can consider

$$\begin{gathered}\int_0^{\xi}W\sqrt{\mathbb{M}\Delta_0\mathscr{G}_0(\xi_1,0)}\left[1+\frac{\mathrm{i}}{\lambda_0}Y_{\xi,0}(\xi_1,0)\right]^{\frac{1}{2}}\mathrm{d}\xi_1\\ \Updownarrow\\ \mathrm{e}^{\frac{\mathrm{i}\pi}{4}}\frac{2(1-\lambda_0)\mathbb{m}\hat{\mathbb{m}}}{\pi}\int_{\hat{\xi}_0}^{\hat{\xi}}\frac{\hat{\xi}_1^{\frac{1}{2}}\left[1+\hat{\eta}_{\mathrm{T}}'^2(\hat{\xi}_1)\right]^{\frac{1}{4}}}{[\hat{\xi}_1^2+\hat{\eta}_{\mathrm{T}}^2(\hat{\xi}_1)]^{\frac{3}{4}}}\mathrm{d}\hat{\xi}_1.\end{gathered}$$

In view of the property of $\hat{\eta}_{\mathrm{T}}(\hat{\xi})$ shown by (3.6), one may conclude that

$$\mathrm{e}^{-\mathrm{i}\frac{\hat{\chi}(\hat{\xi})}{\sqrt{\epsilon\hat{\Gamma}}}}\Longleftrightarrow\mathrm{e}^{-\mathrm{i}\frac{\chi(\xi)}{\sqrt{\epsilon\hat{\Gamma}}}}.$$

https://doi.org/10.1017/S0956792515000066 Published online by Cambridge University Press

Hence, from the matching conditions of the outer solution with the inner solution it follows that

$$\delta(\epsilon)\hat{b}_{*0}(\epsilon)\exp\left\{\frac{-\mathrm{i}}{\sqrt{\epsilon\hat{\Gamma}}}\mathrm{e}^{\frac{\mathrm{i}\pi}{4}}\frac{2(1-\lambda_0)\mathbb{m}}{\pi}\int_0^{\frac{1}{\delta}}\frac{\hat{\xi}_1^{\frac{1}{2}}\left[1+\hat{\eta}_{\mathrm{T}}'^2(\hat{\xi}_1)\right]^{\frac{1}{4}}}{[\hat{\xi}_1^2+\hat{\eta}_{\mathrm{T}}^2(\hat{\xi}_1)]^{\frac{3}{4}}}\mathrm{d}\hat{\xi}_1\right\}=\epsilon,$$
$$\hat{d}_2=-\bar{h}_1(0).$$

It is then derived that in the far field of the root region, the root solution gives

$$\delta(\epsilon)\hat{\mathbb{h}}_{*0}=-\epsilon\Delta(\epsilon)\bar{h}_1(0)\hat{H}_2(\hat{\xi})+\cdots, \tag{4.34}$$

where

$$\Delta(\epsilon)=\exp\left\{\frac{\mathrm{e}^{\frac{\mathrm{i}3\pi}{4}}}{\sqrt{\epsilon\hat{\Gamma}}}\frac{2(1-\lambda_0)\mathbb{m}}{\pi}\int_0^{\frac{1}{\delta}}\frac{\hat{\xi}_1^{\frac{1}{2}}\left[1+\hat{\eta}_{\mathrm{T}}'^2(\hat{\xi}_1)\right]^{\frac{1}{4}}}{[\hat{\xi}_1^2+\hat{\eta}_{\mathrm{T}}^2(\hat{\xi}_1)]^{\frac{3}{4}}}\mathrm{d}\hat{\xi}_1\right\}.$$

As $\epsilon\to 0$, the pre-factor $\Delta(\epsilon)\to 0$ is exponentially decaying.

4.3 Root inner solution in the sub-region (I)

In the sub-region (I), which contains the bottom of the root region ($\hat{\xi}=\hat{\eta}=0$), the physical solution $\Re\{\hat{\mathbb{h}}_{*0}(\hat{\xi})\}$ in the root region must satisfy the smoothness conditions at the bottom ($\hat{\xi}=0,\hat{\eta}=\hat{\eta}_{\mathrm{b}}$):

$$\Re\{\hat{\mathbb{h}}_{*0}(0)\}=\Re\{\hat{\mathbb{h}}_{*0}'(0)\}=0. \tag{4.35}$$

As a consequence, the root solution must have the form:

$$\hat{\mathbb{h}}_{*0}(\hat{\xi})=\tilde{d}_1\hat{H}_1(\hat{\xi})+\tilde{d}_2\hat{H}_2(\hat{\xi}) \tag{4.36}$$

with $\tilde{d}_1$ and $\tilde{d}_2$ both nonzero. Now the questions are raised as to how does the asymptotic solution (4.36), which comprises two waves in the sub-region (I) near the bottom of the root, connect with the asymptotic solution (4.34), which solely comprises one wave in the far filed of the root region, sub-region (II)? how does the root solution behave in the transition region? The key to answer these questions is that the above obtained asymptotic solutions have a *simple turning point singularity*. To explore such a singularity, very similar to the system of dendritic growth [23–25], one needs to study the problem in the complex ξ-plane, and extend all the functions depending on the real variable $\hat{\xi}$, such as the wave number function $\hat{k}_s$, $\hat{\mathbb{h}}_{*0}$, $\hat{C}_{*0}$, etc, to the corresponding complex functions by analytical continuation. It is noted from (4.24) that the wave number function has a complex root $\hat{k}_s(\hat{\xi}_c)=0$. Indeed, from the property of $\hat{\eta}_{\mathrm{T}}(\hat{\xi})$ shown by (3.6), we may approximately write $\hat{\eta}_{\mathrm{T}}(\hat{\xi})=\hat{P}_3(\hat{\xi})$ in the root region $\hat{\xi}=O(1)$. By setting $\left[1+\hat{\eta}_{\mathrm{T}}'^2(\hat{\xi}_c)\right]=1+(2\mathbb{o}_2\hat{\xi}_c+3\mathbb{o}_3\hat{\xi}_c^2)^2=0$, we derive the complex turning points

$$\hat{\xi}_c=\frac{-2\mathbb{o}_2\pm\sqrt{4\mathbb{o}_2^2+12\ \mathrm{i}\mathbb{o}_3}}{6\mathbb{o}_3}, \tag{4.37}$$

https://doi.org/10.1017/S0956792515000066 Published online by Cambridge University Press

which are the functions of joint point of $\hat{\xi}_*$. Among the above two roots, we take the one with the minus sign, such $\hat{\xi}_c$ is located in the fourth quarter of the complex $\hat{\xi}$ plane with $\Re\{\hat{\xi}_c\} > 0, \Im\{\hat{\xi}_c\} < 0$, as shown in Figure 10.

The presence of the turning point $\hat{\xi}_c$ plays a crucial role for the interface closure. According to the turning point theory, the complex $\hat{\xi}$ plane will be divided by the Stokes lines and anti-Stokes lines emitted from $\hat{\xi}_c$ into several sectors. In each sector, the pair of coefficients $(\tilde{d}_1, \tilde{d}_2)$ may have different values. To determine the connection condition of these coefficients, one needs to study the properties of the turning point singularity and derive the inner-inner equation in the vicinity of $(\hat{\xi}_c, 0)$ in the extended complex plane $(\tilde{\xi}, \hat{\eta})$ and find its solutions.

5 The inner-inner equation in the vicinity of $(\hat{\xi}_c, 0)$

We introduce the following inner-inner variables in the vicinity of $(\hat{\xi}_c, 0)$, as it was done in [23–25], which we call the sub-domain (T):

$$\tilde{\xi}_* = \frac{(\hat{\xi} - \hat{\xi}_c)}{(\epsilon\hat{\Gamma})^{\hat{\alpha}}}, \quad \tilde{\eta}_* = \frac{\hat{\eta}}{(\epsilon\hat{\Gamma})^{\hat{\alpha}}}. \tag{5.1}$$

It is evident that in the sub-domain (T), the SPE part of root solution does not have multiple length scales and cannot be expressed in the form of multiple variables. To derive the system valid in the sub-domain (T), one needs to start with the system (4.5)–(4.7). Now, denote the SPE-part of the root solution in sub-domain (T) by

$$\tilde{C}_*(\tilde{\xi}_*, \tilde{\eta}_*, \epsilon) = \hat{C}_{\mathrm{S}}(\hat{\xi}, \hat{\eta}, \epsilon), \quad \tilde{h}_*(\tilde{\xi}_*, \epsilon) = \hat{\eta}_{\mathrm{S}}(\hat{\xi}, \epsilon). \tag{5.2}$$

By neglecting the higher order terms, as the leading order approximation in the vicinity of the turning point, $\{\tilde{C}_*(\tilde{\xi}_*, \tilde{\eta}_*, \epsilon) \approx \tilde{C}_{*0}(\tilde{\xi}_*, \tilde{\eta}_*), \tilde{h}_*(\tilde{\xi}_*, \epsilon) \approx \tilde{h}_{*0}(\tilde{\xi}_*)\}$ is subject to the following inner-inner equation:

$$\frac{\partial^2 \tilde{C}_{*0}}{\partial \tilde{\xi}_*^2} + \left[1 + \hat{\eta}_{\mathrm{T}}'^2(\hat{\xi})\right] \frac{\partial^2 \tilde{C}_{*0}}{\partial \tilde{\eta}_*^2} - 2\hat{\eta}_{\mathrm{T}}'(\hat{\xi}) \frac{\partial^2 \tilde{C}_{*0}}{\partial \tilde{\eta}_* \partial \tilde{\xi}_*} = 0. \tag{5.3}$$

We consider the following type of the solutions for $\tilde{C}_{*0}$:

$$\tilde{C}_{*0} = \tilde{A}_{*0} \exp\left\{\mathrm{i}\tilde{\xi}_* - \tilde{\lambda}_c \tilde{\eta}_*\right\}. \tag{5.4}$$

By substituting (5.4) into (5.3), it is obtained that

$$-1 + \tilde{\lambda}_c^2(1 + \hat{\eta}_{\mathrm{T}}'^2) + \mathrm{i}2\hat{\eta}_{\mathrm{T}}'(\hat{\xi})\tilde{\lambda}_c = 0,$$

and

$$\tilde{\lambda}_c = \frac{1}{1 + \mathrm{i}\hat{\eta}_{\mathrm{T}}'(\hat{\xi})}, \quad (\Re\{\tilde{\lambda}_c\} > 0). \tag{5.5}$$

https://doi.org/10.1017/S0956792515000066 Published online by Cambridge University Press

From (5.4), one may deduce that

$$\frac{\partial \tilde{C}_{*0}}{\partial \tilde{\eta}_*} = \mathrm{i}\tilde{\lambda}_c \frac{\partial \tilde{C}_{*0}}{\partial \tilde{\xi}_*}. \tag{5.6}$$

Furthermore, in the leading order approximation, it is derived that $\tilde{C}_{*0} = O(\epsilon \tilde{h}_{*0})$ and the interface conditions at the interface at $\tilde{\eta}_* = 0$ are:

$$\tilde{C}_{*0} = \frac{1}{\mathbb{M}W \hat{\mathscr{G}}_0(\hat{\xi}, 0)} \frac{\partial^2 \tilde{h}_{*0}}{\partial \tilde{\xi}_*^2}, \tag{5.7}$$

$$\frac{\partial \tilde{C}_{*0}}{\partial \tilde{\eta}_*} - \frac{\partial \bar{\mathbb{C}}_{*1}}{\partial \hat{\xi}} \frac{\partial \tilde{h}_{*0}}{\partial \tilde{\xi}_*} - W(1-\kappa) y_{*0} \hat{Y}_{0,\hat{\xi}}(\hat{\xi}, 0) \frac{\partial \tilde{h}_{*0}}{\partial \tilde{\xi}_*} = 0. \tag{5.8}$$

By applying the relationship (5.6), from (5.8) we derive that

$$\mathrm{i}\tilde{\lambda}_c \frac{\partial \tilde{C}_{*0}}{\partial \tilde{\xi}_*} - W\left[(1-\kappa) y_{*0} - \lambda_{\mathrm{G}}\right] \hat{Y}_{\hat{\xi},0}(\hat{\xi}, 0) \frac{\partial \tilde{h}_{*0}}{\partial \tilde{\xi}_*} = 0. \tag{5.9}$$

By combining (5.9) with (5.7), we derive

$$\mathrm{i}\tilde{\lambda}_c \frac{1}{\mathbb{M}W \hat{\mathscr{G}}_0(\hat{\xi}, 0)} \frac{\partial^3 \tilde{h}_{*0}}{\partial \tilde{\xi}_*^3} - W\left[(1-\kappa) y_{*0} - \lambda_{\mathrm{G}}\right] \hat{Y}_{\hat{\xi},0}(\hat{\xi}, 0) \frac{\partial \tilde{h}_{*0}}{\partial \tilde{\xi}_*} = 0, \tag{5.10}$$

which can be re-written as

$$\frac{\partial^3 \tilde{h}_{*0}}{\partial \tilde{\xi}_*^3} + \tilde{k}_s^2(\hat{\xi}) \frac{\partial \tilde{h}_{*0}}{\partial \tilde{\xi}_*} = 0. \tag{5.11}$$

In (5.11), we have defined

$$\hat{k}_s^2(\hat{\xi}) = \mathrm{i}\mathbb{m}^2 \hat{\mathscr{G}}_0(\hat{\xi}, 0) \hat{Y}_{\hat{\xi},0}(\hat{\xi}, 0)\left[1 + \mathrm{i}\hat{\eta}'_{\mathrm{T}}(\hat{\xi})\right],$$

so that

$$\hat{k}_s(\hat{\xi}) = \mathrm{e}^{\frac{\mathrm{i}\pi}{4}} \frac{2(1-\lambda_0)\mathbb{m}}{\pi} \frac{\hat{\xi}^{\frac{1}{2}}}{\left[\hat{\xi}^2 + \hat{\eta}_{\mathrm{T}}^2(\hat{\xi})\right]^{\frac{3}{4}}} \left[1 + \mathrm{i}\hat{\eta}'_{\mathrm{T}}(\hat{\xi})\right]^{\frac{1}{2}}. \tag{5.12}$$

It is seen that at $\hat{\xi} = \hat{\xi}_c$, we have $\hat{k}_s(\hat{\xi}_c) = 0$ since $\left[1 + \mathrm{i}\hat{\eta}'_{\mathrm{T}}(\hat{\xi}_c)\right] = 0$. Moreover, one can write that as $\hat{\xi} \to \hat{\xi}_c$

$$\hat{k}_s^2(\hat{\xi}) = \mathscr{A}^2(\hat{\xi} - \hat{\xi}_c) + O(\text{h.o.t}),$$

where

$$\begin{aligned} \mathscr{A}^2 &= \mathrm{i}\frac{4(1-\lambda_0)^2 \mathbb{m}^2}{\pi^2} \frac{\hat{\xi}_c}{\left[\hat{\xi}_c^2 + \hat{\eta}_{\mathrm{T}}^2(\hat{\xi}_c)\right]^{\frac{3}{2}}} \left[\mathrm{i}\hat{\eta}''_{\mathrm{T}}(\hat{\xi}_c)\right] \\ &= -\frac{4(1-\lambda_0)^2 \mathbb{m}^2}{\pi^2} \frac{\hat{\xi}_c}{\left[\hat{\xi}_c^2 + \hat{\eta}_{\mathrm{T}}^2(\hat{\xi}_c)\right]^{\frac{3}{2}}} (2\mathbb{a}_2 + 6\mathbb{a}_3 \hat{\xi}_c). \end{aligned} \tag{5.13}$$

https://doi.org/10.1017/S0956792515000066 Published online by Cambridge University Press

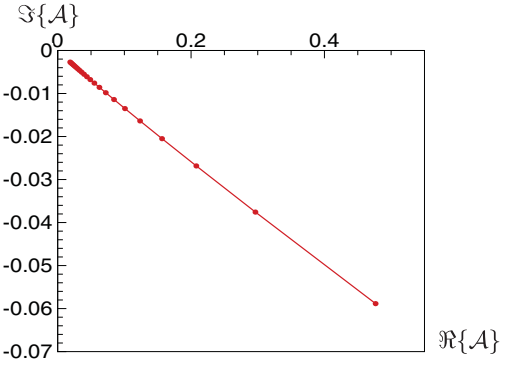

FIGURE 7. The variation of the coefficient $\mathscr{A}$ on the complex $\mathscr{A}$-plane with the parameter $\hat{\tilde{\xi}}_*$ for the typical case: $\alpha = 0.88, \mathbb{o} = 2.63, \kappa = 0.1, \lambda_0 = 0.6, \lambda_G = 2, \mathbb{M} = 1$. $\Re\{\mathscr{A}\}$ decreases when $\hat{\tilde{\xi}}_*$ increases from $0.5 \to 5.0$ with the step size $\Delta\hat{\tilde{\xi}}_* = 0.2$. The argument $\arg\{\mathscr{A}\} \approx -0.04\pi$.

The variation of $\mathscr{A}$ in the complex plane with $\hat{\tilde{\xi}}_*$ for a typical case is shown in Figure 7. We derive

$$\hat{k}_s^2(\hat{\xi}) \approx \mathscr{A}^2(\epsilon\hat{\Gamma})^{\hat{\alpha}}\tilde{\xi}_*.$$

As a consequence, in the leading order approximation (5.11) is reduced to:

$$(\epsilon\hat{\Gamma})^{1-2\hat{\alpha}}\frac{\mathrm{d}^2 W_{*0}}{\mathrm{d}\tilde{\xi}_*^2} + (\epsilon\hat{\Gamma})^{\hat{\alpha}}\mathscr{A}^2\tilde{\xi}_* W_{*0} = 0. \tag{5.14}$$

Here we write $W_{*0}(\tilde{\xi}_*) = \frac{\mathrm{d}\hat{\mathbb{h}}_{*0}}{\mathrm{d}\tilde{\xi}_*}(\tilde{\xi}_*)$. By setting $\hat{\alpha} = \frac{1}{3}$, we derive the Airy equation:

$$\frac{\mathrm{d}^2 W_{*0}}{\mathrm{d}\tilde{\xi}_*^2} + \mathscr{A}^2\tilde{\xi}_* W_{*0} = 0. \tag{5.15}$$

Furthermore, by letting

$$\overline{\xi}_* = \mathscr{A}^{\frac{2}{3}}\tilde{\xi}_* = \mathscr{A}^{\frac{2}{3}}\frac{(\hat{\xi} - \hat{\xi}_c)}{(\epsilon\hat{\Gamma})^{\frac{1}{3}}},$$

one may further change (5.15) into the standard form of Airy equation:

$$\frac{\mathrm{d}^2 W_{*0}}{\mathrm{d}\overline{\xi}_*^2} + \overline{\xi}_* W_{*0} = 0. \tag{5.16}$$

It is now seen clearly that the system has a simple turning point singularity at $\hat{\xi} = \hat{\xi}_c$, or $\overline{\xi}_* = 0$. According to the turning point theory, one can draw three Stokes lines and anti-Stokes lines emitted from $\hat{\xi}_c$ on the complex $\hat{\xi}_c$ plane. Among these lines, the anti-Stokes line (A_1) divides the complex $\hat{\xi}_c$ plane into two sectors: (S_1) and (S_2), and intersects the real $\hat{\xi}$-axis at $\hat{\xi}_c'$. The intersection point $\hat{\xi}_c'$ divides the real $\hat{\xi}$-axis into two subintervals $(0, \hat{\xi}_c')$ and $(\hat{\xi}_c', \infty)$. The pair of the constants $(\tilde{d}_1, \tilde{d}_2)$ in (4.28) will have different values in the sectors (S_1) and (S_2), so does in the sub-intervals $(0, \hat{\xi}_c')$ and $(\hat{\xi}_c', \infty)$.

The open angle between two neighbouring Stokes lines and two neighbouring anti-Stakes lines emitted from the turning point $\hat{\xi}_c$ is $\theta = \frac{2}{1+2}\pi = \frac{2}{3}\pi$, as shown in Figure 8.

https://doi.org/10.1017/S0956792515000066 Published online by Cambridge University Press

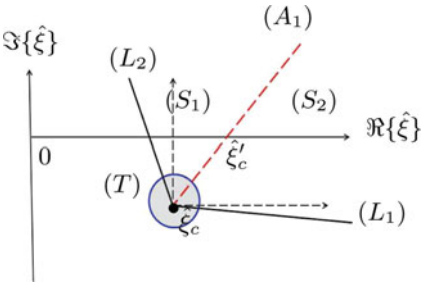

FIGURE 8. The sketch of the structure of Stokes and anti-Stokes lines emitted from the turning point $\hat{\xi}_c$ in the root region, where (T) is the vicinity of the turning point $\hat{\xi}_c$, (L_1) and (L_2) are the Stokes lines, while (A_1) is the anti-Stokes line.

The general solution of (5.16) is

$$W_{*0}(\overline{\xi}_*) = D_{*1}\overline{\xi}_*^{\frac{1}{2}} H_{\frac{1}{3}}^{(1)}(\zeta) + D_{*2}\overline{\xi}_*^{\frac{1}{2}} H_{\frac{1}{3}}^{(2)}(\zeta), \quad \left(\zeta = \frac{2}{3}\overline{\xi}_*^{\frac{3}{2}}\right), \tag{5.17}$$

where $H_{\frac{1}{3}}^{(1)}(\zeta)$ is the Hankel function of the first kind of order $\frac{1}{3}$, while $H_{\frac{1}{3}}^{(2)}(\zeta)$ is the Hankel function of the second kind of order $\frac{1}{3}$.

6 Matching

Away from the turning point $\hat{\xi} = \hat{\xi}_c$, the inner-inner solution in the sub-domain (T) must match with the root solution in the sector (S_2), as well as the root solution in the sector (S_2). The matching conditions will determine the unknown coefficients in the root solutions and leads to a quantization condition for the eigenvalue $\hat{\xi}_*$

6.1 Inner-inner solutions in sub-domain (T) matching with the root solution in sector (S_2)

We now let $\overline{\xi}_* \to \infty$ starting from the turning point $\overline{\xi}_* = 0$ in sector (S_2). From the solution (5.17), we derive that in the domain $(S_2)\bigcap(T)$, we have $D_{*1} = 0$, and the inner-inner solution can be written as

$$W_{*0}(\overline{\xi}_*) = D_{*2}\overline{\xi}_*^{\frac{1}{2}} H_{\frac{1}{3}}^{(2)}(\zeta). \tag{6.1}$$

Hence, as $\overline{\xi}_* \to \infty$, we have

$$W_{*0}(\overline{\xi}_*) = W_{*0}^{(\mathrm{T})} = D_{*2}\mathrm{e}^{\mathrm{i}(5/12)\pi}\sqrt{\frac{2}{\pi\zeta}}\mathrm{e}^{-\mathrm{i}\zeta},$$

and

$$D_{*2}\mathrm{e}^{\mathrm{i}(5/12)\pi} = -\epsilon\Delta(\epsilon)h_1(0), \tag{6.2}$$

https://doi.org/10.1017/S0956792515000066 Published online by Cambridge University Press

which may be considered as an incoming W-wave in the sector (S_2). The root solution in the section (II) can be finally written as

$$\begin{aligned}\hat{\eta}_{\mathrm{B}}(\hat{\xi},\epsilon) &= \delta(\epsilon)\hat{\eta}_{\mathrm{T}}(\hat{\xi}) - \epsilon\Delta(\epsilon)h_1(0)\hat{H}_2(\hat{\xi}) + \cdots \\ &= \delta(\epsilon)\hat{\eta}_{\mathrm{T}}(\hat{\xi}) - \epsilon h_1(0)\exp\left\{\frac{\mathrm{e}^{\frac{\mathrm{i}3\pi}{4}}}{\sqrt{\epsilon\hat{\Gamma}}}\frac{2(1-\lambda_0)\mathbb{m}}{\pi}\int_{\hat{\xi}}^{\frac{1}{\delta}}\frac{\hat{\xi}_1^{\frac{1}{2}}\left[1+\hat{\eta}_{\mathrm{T}}'^2(\hat{\xi}_1)\right]^{\frac{1}{4}}}{\left[\hat{\xi}_1^2+\hat{\eta}_{\mathrm{T}}^2(\hat{\xi}_1)\right]^{\frac{3}{4}}}\mathrm{d}\hat{\xi}_1\right\} \\ &\quad +\epsilon\delta(\epsilon)\bar{h}_{*0}(\hat{\xi}) + \cdots .\end{aligned} \tag{6.3}$$

6.2 Inner-inner solutions in sub-domain (T) matching with the root solution in sector (S_1)

In the sector (S_1), according to the theory of Hankel functions, one has the formula:

$$H_{\frac{1}{3}}^{(2)}(\zeta\mathrm{e}^{\mathrm{i}\pi}) = H_{\frac{1}{3}}^{(2)}(\zeta) + \mathrm{e}^{\mathrm{i}\frac{1}{3}\pi}H_{\frac{1}{3}}^{(1)}(\zeta), \quad (-\pi < \arg(\zeta) \leqslant \pi).$$

Hence, it is deduced that the inner-inner solution (6.1) in $(S_1)\bigcap(T)$ can be expressed in the following form:

$$W_{*0}(\overline{\xi}_*) = D_{*2}\overline{\xi}_*^{\frac{1}{2}}\left[H_{\frac{1}{3}}^{(2)}(\zeta) + \mathrm{e}^{\mathrm{i}\pi/3}H_{\frac{1}{3}}^{(1)}(\zeta)\right]. \tag{6.4}$$

Thus, letting $\overline{\xi}_* \to \infty$ in the sector (S_1), we obtain

$$\begin{aligned}W_{*0}(\overline{\xi}_*) &= D_{*2}\left[\sqrt{\frac{2}{\pi\zeta}}\mathrm{e}^{-\mathrm{i}\zeta+\mathrm{i}(5/12)\pi} + \mathrm{e}^{\mathrm{i}\pi/3}\sqrt{\frac{2}{\pi\zeta}}\mathrm{e}^{\mathrm{i}\zeta-\mathrm{i}(5/12)\pi}\right] \\ &= -\epsilon\Delta(\epsilon)h_1(0)\sqrt{\frac{2}{\pi\zeta}}\left[\mathrm{e}^{-\mathrm{i}\zeta} - \mathrm{i}\mathrm{e}^{\mathrm{i}\zeta}\right] \\ &= \tilde{b}_2 W_{*0}^{(-)}(\hat{\xi}) + \tilde{b}_1 W_{*0}^{(+)}(\hat{\xi}),\end{aligned} \tag{6.5}$$

where $\tilde{b}_2/\tilde{b}_1 = \mathrm{i}$.

On the other hand, for the inner-inner solution (4.36) in the sector (S_1),

$$\hat{\mathbb{h}}_{*0}(\hat{\xi}) = \tilde{d}_1\hat{H}_1(\hat{\xi}) + \tilde{d}_2\hat{H}_2(\hat{\xi}), \tag{6.6}$$

where the fundamental solutions $\hat{H}_1(\hat{\xi})$ and $\hat{H}_2(\hat{\xi})$ can be specified as

$$\hat{H}_1(\hat{\xi}) = \exp\left\{\frac{\mathrm{i}}{\sqrt{\epsilon\hat{\Gamma}}}\int_{\hat{\xi}_c}^{\hat{\xi}}\hat{k}_s(\hat{\xi}_1)\mathrm{d}\hat{\xi}_1\right\}, \quad \hat{H}_2(\hat{\xi}) = \exp\left\{-\frac{\mathrm{i}}{\sqrt{\epsilon\hat{\Gamma}}}\int_{\hat{\xi}_c}^{\hat{\xi}}\hat{k}_s(\hat{\xi}_1)\mathrm{d}\hat{\xi}_1\right\},$$

by setting the lower limit $a = \hat{\xi}_c$. Moreover, one may express it in terms of the W-wave representation as

$$\hat{W}_{*0}(\hat{\xi}) = \tilde{d}_1\hat{W}_{*0}^{(+)}(\hat{\xi}) + \tilde{d}_1\hat{W}_{*0}^{(-)}(\hat{\xi}), \tag{6.7}$$

where

$$\hat{W}_{*0}(\hat{\xi}) = \hat{\mathbb{h}}_{*0}'(\hat{\xi}), \quad \hat{W}_{*0}^{(+)}(\hat{\xi}) = \hat{H}_1'(\hat{\xi}), \quad \hat{W}_{*0}^{(-)}(\hat{\xi}) = \hat{H}_2'(\hat{\xi}).$$

https://doi.org/10.1017/S0956792515000066 Published online by Cambridge University Press

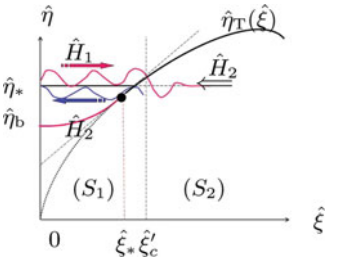

FIGURE 9. The sketch of wave diagram with W-wave representation in the root region.

By comparing (6.5) with (6.7) and noting that

$$\begin{array}{lll} W^{(+)}_{*0}(\hat{\xi}) & \text{outgoing W-wave with } \tilde{k}_s & \Longleftrightarrow \hat{W}^{(+)}_{*0}(\hat{\xi}) \quad \text{W-wave with } \hat{k}_s, \\ W^{(-)}_{*0}(\hat{\xi}) & \text{incoming W-wave with } -\tilde{k}_s & \Longleftrightarrow \hat{W}^{(-)}_{*0}(\hat{\xi}) \quad \text{W-wave with } -\hat{k}_s, \end{array}$$

it is deduced that in order for the inner solution in the vicinity of turning point (T) to match with the root solution in the sector (S_1), the connection conditions:

$$\tilde{d}_2 = -\epsilon\Delta(\epsilon)h_1(0); \quad \tilde{d}_2/\tilde{d}_1 = \tilde{b}_2/\tilde{b}_1 = \mathrm{i}, \quad \tilde{d}_1 = -\mathrm{i}$$

must be satisfied. As a consequence, root solution in the sector (S_1) (4.36) becomes

$$\hat{\mathbb{h}}_{*0}(\hat{\xi}) = \tilde{d}_2 \left[\hat{H}_2(\hat{\xi}) - \mathrm{i}\hat{H}_1(\hat{\xi})\right]. \tag{6.8}$$

7 The quantization condition for the eigenvalue $\hat{\xi}_*$

From (6.8), the corresponding physical solution in the sector (S_1) $(0 \leqslant \hat{\xi} \leqslant \hat{\xi}'_c)$ is derived as

$$\hat{\mathbb{h}}_{*0}(\hat{\xi}) = \tilde{d}_2 \Re\left\{\hat{H}_2(\hat{\xi}) - \mathrm{i}\hat{H}_1(\hat{\xi})\right\}, \tag{7.1}$$

which should satisfy the root conditions at the bottom of the root region $(\hat{\xi} = 0, \hat{\eta} = \hat{\eta}_{\mathrm{b}})$:

$$\hat{\mathbb{h}}_{*0}(0) = 0, \quad \hat{\mathbb{h}}'_{*0}(0) = 0. \tag{7.2}$$

The behaviour of the solution over the interval $(0 \leqslant \hat{\xi} < \hat{\xi}'_c)$ has a similarity to the Schrödinger waves trapped in a finite potential well $\hat{\eta}_{\mathrm{T}}(\hat{\xi})$ in quantum mechanics, as sketched in Figure 9. The waves in the sub-region (S_1) are trapped between the bottom of root $\hat{\xi} = 0$ and the reflection point ξ'_c. Such a wave diagram may be called *the trapped-waves mechanism*, which was first discovered in the system of dendritic growth (see [23–25]. Despite of the above similarity, the substantial difference in mathematics between two phenomena should not be under-estimated. In the problem of quantum mechanism, the turning point lies on the real axis, whereas in the problem under study, the turning point lies on the complex plane away from the real axis. Hence, the deduction of the pre-factor 'i' existing in (7.1) is not trivial.

https://doi.org/10.1017/S0956792515000066 Published online by Cambridge University Press

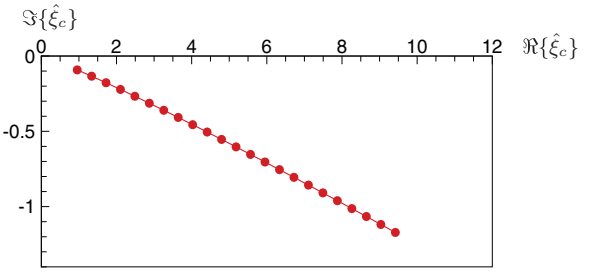

FIGURE 10. The variation of the turning point $\hat{\xi}_c$ on the complex $\hat{\xi}_c$-plane with the parameter $\hat{\xi}_*$ for the typical case: $\alpha = 0.88, \mathbb{o} = 2.63, \kappa = 0.1, \lambda_0 = 0.6, \lambda_G = 2, \mathbb{M} = 1$. $\Re\{\hat{\xi}_c\}$ increases when $\hat{\xi}_*$ increases from $0.5 \to 5.0$ with the step size $\Delta\hat{\xi}_* = 0.2$.

Due to $H_1'(0) = H_3'(0) = 0$, the smoothness condition $\hat{\mathbb{h}}'_{*0}(0) = 0$ is always satisfied. To satisfy the condition $\hat{\mathbb{h}}_{*0}(0) = 0$, we require

$$\Re[\hat{H}_2(0) - \mathrm{i}\hat{H}_1(0)] = 0. \tag{7.3}$$

Recalling (see (4.19), (4.24)) that

$$\begin{aligned}\hat{\chi}(\hat{\xi}) &= \int_{\hat{\xi}_c}^{\hat{\xi}} \hat{k}_s(\hat{\xi}_1)\mathrm{d}\hat{\xi}_1 = \hat{\chi}_{\mathrm{R}}(\hat{\xi}) + \mathrm{i}\hat{\chi}_{\mathrm{I}}(\hat{\xi}) \\ &= \frac{2(1-\lambda_0)\mathbb{m}}{\pi} \int_{\hat{\xi}_c}^{\hat{\xi}} \left[\frac{\mathrm{i}}{\lambda_c(\hat{\xi}_1)+\mathrm{i}}\right]^{\frac{1}{2}} \frac{\hat{\xi}_1^{\frac{1}{2}}(1+\hat{\eta}_{\mathrm{T}}'^2)^{\frac{1}{4}}}{[\hat{\xi}_1^2+\hat{\eta}_{\mathrm{T}}^2(\hat{\xi}_1)]^{\frac{3}{4}}}\mathrm{d}\hat{\xi}_1,\end{aligned} \tag{7.4}$$

we define

$$\begin{aligned}\hat{Q}_{\mathrm{R}} &= -\frac{\hat{\chi}_{\mathrm{R}}(0)}{\sqrt{\epsilon\hat{\Gamma}}} = \frac{2}{\sqrt{\epsilon\hat{\Gamma}}}\frac{(1-\lambda_0)\mathbb{m}}{\pi}\Re\left\{\int_0^{\hat{\xi}_c}\left[\frac{\mathrm{i}}{\lambda_c(\hat{\xi}_1)+\mathrm{i}}\right]^{\frac{1}{2}}\frac{\hat{\xi}_1^{\frac{1}{2}}\left[1+\hat{\eta}_{\mathrm{T}}'^2(\hat{\xi}_1)\right]^{\frac{1}{4}}}{[\hat{\xi}_1^2+\hat{\eta}_{\mathrm{T}}^2(\hat{\xi}_1)]^{\frac{3}{4}}}\mathrm{d}\hat{\xi}_1\right\}, \\ \hat{Q}_{\mathrm{I}} &= -\frac{\hat{\chi}_{\mathrm{I}}(0)}{\sqrt{\epsilon\hat{\Gamma}}} = \frac{2}{\sqrt{\epsilon\hat{\Gamma}}}\frac{(1-\lambda_0)\mathbb{m}}{\pi}\Im\left\{\int_0^{\hat{\xi}_c}\left[\frac{\mathrm{i}}{\lambda_c(\hat{\xi}_1)+\mathrm{i}}\right]^{\frac{1}{2}}\frac{\hat{\xi}_1^{\frac{1}{2}}\left[1+\hat{\eta}_{\mathrm{T}}'^2(\hat{\xi}_1)\right]^{\frac{1}{4}}}{[\hat{\xi}_1^2+\hat{\eta}_{\mathrm{T}}^2(\hat{\xi}_1)]^{\frac{3}{4}}}\mathrm{d}\hat{\xi}_1\right\}.\end{aligned} \tag{7.5}$$

The bottom smoothness condition (7.3) finally yields the quantization condition

$$\mathrm{e}^{2\hat{Q}_{\mathrm{R}}} = \cot\hat{Q}_{\mathrm{I}}. \tag{7.6}$$

Note that $\hat{Q} = \hat{Q}_{\mathrm{R}} + \mathrm{i}Q_{\mathrm{I}}$ is a composed function of $\hat{\xi}_*$, since the turning point $\hat{\xi}_c$ is a complex function of the joint point $\hat{\xi}_*$. The quantization condition (7.6), which modifies the result given in [11], yields a single eigenvalue $\hat{\xi}_*$ as the function of ϵ and other the thermodynamic properties of the system, as well as the growth conditions. For the typical case: $\epsilon = 0.1$, $\kappa = 0.1$, $\lambda_G = 2.0$, $\lambda_0 = 0.6$, $W_0 = 1.745$, $\mathbb{M} = 1.0, \hat{\Gamma} = 1.0$, from the quantization condition (7.6), we calculate that $\hat{\xi}_* = 2.14$, $\Re\{\hat{\xi}_c\} = 4.11, \Im\{\hat{\xi}_c\} = -0.466$.

The variations of eigenvalue $\hat{\xi}_*$ with ϵ are shown in Figure 11(a) for the typical cases $\hat{\Gamma} = 1.0, 1.5, 2.0$. The outer solutions for these cases yield $\alpha \approx 0.88$ and $\mathbb{o}_0 \approx 2.63$. These parameters are rather insensitive to the parameter κ and $\hat{\Gamma}$. It is seen that the value

https://doi.org/10.1017/S0956792515000066 Published online by Cambridge University Press

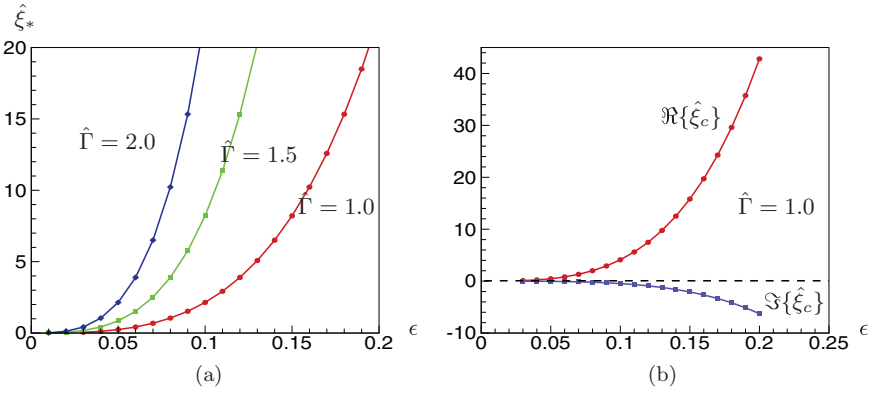

FIGURE 11. For the cases of $\kappa = 0.1$, $\lambda_0 = 0.6$, $W_0 = 1.7453$, $\mathbb{M} = 1.0$, $\lambda_G = 2.0$, (a) the variations of $\hat{\bar{\xi}}_*$ with the parameter ϵ; (b) the variations of $\Re\{\hat{\bar{\xi}}_c\}$ and $\Im\{\hat{\bar{\xi}}_c\}$ with the parameter ϵ. The calculations have been done using the outer solutions for these cases with $\alpha = 0.88$ and $\mathbb{o}_0 = 2.63$.

of $\hat{\bar{\xi}}_*$ increases with increasing surface tension parameter $\hat{\Gamma}$ and Péclet number ϵ. In Figure 11(b) we show variation of the turning point location $\hat{\bar{\xi}}_c$ with the Péclet number ϵ for the case of $\hat{\Gamma} = 1.0$. It is seen that the absolute values of $|\Re\{\hat{\bar{\xi}}_c\}|$ and $|\Im\{\hat{\bar{\xi}}_c\}|$ both increase with increasing Péclet number ϵ, while for a fixed ϵ, $|\Re\{\hat{\bar{\xi}}_c\}| \gg |\Im\{\hat{\bar{\xi}}_c\}|$.

Once $\hat{\bar{\xi}}_*$ is determined, and the parameters $\hat{\eta}_*$ and $\hat{\eta}_b$ are determined, then the inner solution in the whole root region ($0 \leqslant \hat{\bar{\xi}} < \infty$) is determined, and may be written as

$$\hat{\eta}_B(\hat{\bar{\xi}}, \epsilon) = \delta(\epsilon)\hat{\eta}_T(\hat{\bar{\xi}}) - \epsilon\Delta(\epsilon)\bar{h}_1(0)e^{\frac{\hat{\chi}_I(\hat{\bar{\xi}})}{\sqrt{\epsilon\hat{\Gamma}}}}\cos\left(\frac{\hat{\chi}_R(\hat{\bar{\xi}})}{\sqrt{\epsilon\hat{\Gamma}}}\right) + \cdots . \tag{7.7}$$

Together with the outer solution

$$\eta_B(\xi, \epsilon) = \epsilon\left[\bar{h}_1(\xi) - \bar{h}_1(0)e^{\frac{\chi_I(\xi)}{\sqrt{\epsilon\hat{\Gamma}}}}\cos\left(\frac{\chi_R(\xi)}{\sqrt{\epsilon\hat{\Gamma}}}\right)\right] + \cdots , \tag{7.8}$$

the composite solution in the whole physical region, including the outer region and inner region, is derived as

$$\begin{aligned}\eta_B(\xi, \epsilon) = {} & \delta(\epsilon)\hat{\eta}_T(\hat{\bar{\xi}}) - \epsilon\mathbb{o}_0(1+\xi)^\alpha \\ & + \epsilon\left[\bar{h}_1(\xi) - \bar{h}_1(0)e^{\frac{\chi_I(\xi)}{\sqrt{\epsilon\hat{\Gamma}}}}\cos\left(\frac{\chi_R(\xi)}{\sqrt{\epsilon\hat{\Gamma}}}\right)\right] + \cdots .\end{aligned} \tag{7.9}$$

The composite solutions $\eta_B(\xi)$ for $\hat{\Gamma} = 1.0, 1.5, 2.0$ are shown in Figure 12. The global interface shapes on the (X, Y) plane for the cases of $\lambda_0 = 0.4$, $\hat{\Gamma} = 2.0, 3.0, 4.0$ and $\lambda_0 = 0.6$, $\hat{\Gamma} = 1.0, 1.5, 2.0$ are shown in Figures 13(a) and (b), respectively. In the figures, for comparison, we also show the S–T solution with black dashed line and the outer solution with solid red line. It is seen that in the root region the difference between the S–T solution and the solution we obtained is substantial. It is also seen that the effect of surface tension parameter on the pattern formation in the root region is very important. The smaller the value of $\hat{\Gamma}$ the longer the total length of finger.

https://doi.org/10.1017/S0956792515000066 Published online by Cambridge University Press

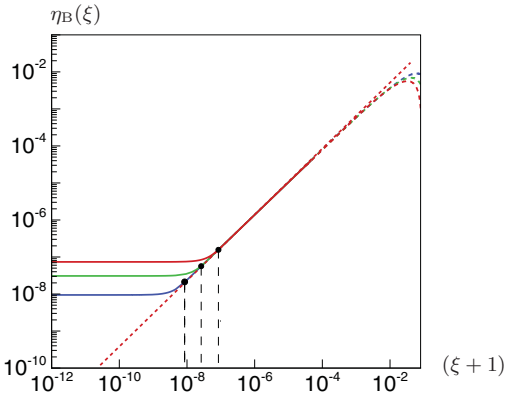

FIGURE 12. The graph of composite solution $\eta_B(\xi)$ in (ξ,η) plane for the typical case: $\epsilon = 0.1$, $\kappa = 0.1$,$\lambda_G = 2.0$, $\lambda_0 = 0.6$, $\mathbb{M} = 1.0$. near $\xi = -1$ for $\hat{\Gamma} = 1.0, 1.5, 2.0$ from bottom to top on the left-hand side of figure. The bullets show the joint points $\hat{\xi}_*$ in the root region. The calculations have been done using the outer solutions for these cases with $\alpha = 0.88$, $\mathbb{o}_0 = 2.63$ and $\delta(\epsilon) = 0.4642\times10^{-8}$.

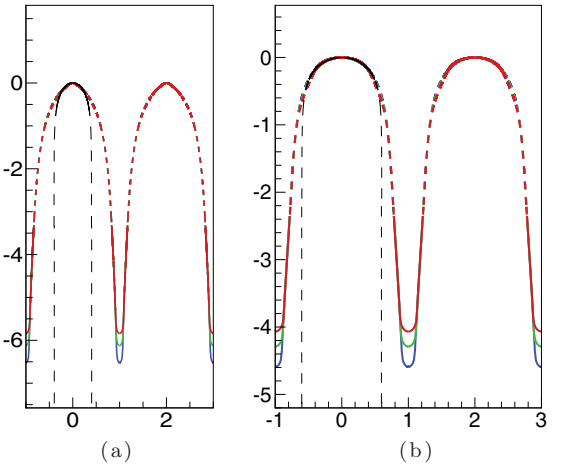

FIGURE 13. The interface shapes drawn on (X, Y) plane for the typical case: $\epsilon = 0.1$, $\kappa = 0.1$, $\mathbb{M} = 1.0$ and (a). $\lambda_0 = 0.4$, $\lambda_G = 0.8$, $\hat{\Gamma} = 2.0, 3.0, 4.0$; (b). $\lambda_0 = 0.6$, $\lambda_G = 2.0$, $\hat{\Gamma} = 1.0, 1.5, 2.0$. It is seen that the total length of finger increases with decreasing value of $\hat{\Gamma}$. In the figures, the black dashed line is given by the Saffman–Taylor solution, the red dashed line is given by the outer solution, which is not valid in the root region, while the solid red line is given by the root solution.

In terms of the global asymptotic solution obtained, we can determine the properties of steady arrayed-cellular growth in the root region and the their dependence on the effects of operating parameters, these properties include: the total length of the finger, Y_b; the mean curvature of the bottom of finger, $\mathscr{K}_b$; the concentration of impurity at the bottom of root, C_{root}. The results are qualitatively consistent with those shown in [11], but there are some quantitative discrepancy between them, due to the correction of the quantization condition. We anticipate that more precise experiments of deep-cellular growth will be performed in the future and the experimental data on these quantities will finally become

https://doi.org/10.1017/S0956792515000066 Published online by Cambridge University Press

available. Thus, one can make the further comparisons of theoretical predictions with experimental data.

8 Conclusions

In this present paper, we investigate the mechanism of interface closure in the root region of the steady state solution for deep-cellular growth. The phenomenon under investigation is determined by a transcendentally small pre-factor beyond all orders. The most important discovery made in the present paper is that the root region comprises three inner-inner layers; the inner system in the root region has a complex turning point $\hat{\xi}_c$ in the extended complex plane whose presence leads to the so-called *trapped-waves mechanism* and plays the crucial role for the interface closure in the root region. The quantization condition derived from the trapped-waves mechanism yields the eigenvalue $\hat{\xi}_*$ as the function of parameter ϵ and other parameters of the system, which determines the total length of the cell hence, the global feature of the interfacial pattern.

It should be remarked that, as described by the solution derived in the present paper, the interface in the root region forms a long and narrow groove. Such a groove looks more like a slender liquid needle, as the width of the groove may be comparable with the thickness of the thin layer. As a consequence, the 2D model adopted in the present paper should be modified in the root region with the inclusion of a 3D effect. Moreover, a steady slender liquid needle may be broken into a sequence of droplets under small perturbations induced by the Rayleigh instability caused by the surface tension. The formation of liquid droplets is indeed observed in some experiments of deep-cellular growth. These issues are worth further investigating in the future.

Acknowledgements

The work is partially supported by the University of Science and Technology, Beijing under the 'Overseas Distinguished Scholar Program' sponsored by the Department of Chinese Education.

References

[1] Rutter, J. W. & Chalmers, B. (1953) A prismatic substructure formed during solidification of metals. *Can. J. Phys.* **31**, 15–39.

[2] Mullins, W.W. & Sekerka, R. F. (1963) Morphological stability of a particle growing by diffusion or heat flow. *J. Appl. Phys.* **34**, 323–329.

[3] Somboonsuk, K., Mason, J. T. & Trivedi, R. (1984) Interdendritc spacing: Part (I)-(II). *Metall. Tran. A* **15**, 967–975; 977–982.

[4] Pelce, P. & Pumir, A. (1985) Cell shape in directional solidification in the small Péclet number limit. *J. Cryst. Growth* **73**, 337–342.

[5] Weeks, J. D. & van-Saarloos, W. (1989) Directional solidification cells with grooves for a small partition coeffcient. *Phy. Rev. A* **39**, 2772–2775.

[6] Ungar, L. H. & Brown, R. A. (1985), Cellular interface morphologies in directional solidification. 4. The formation of deep cells. *Phys. Rev. B* **31,** 5931–5940.

[7] Georgelin, M. & Pocheau, A. (2006) Shape of Growth Cells in Directional Solidifiction, *Phys. Rev. E*, **73**, 011604.
[8] Weeks, J. D., van-Saarloos, W. & Grant, M. (1991) Stability and shape of cellular profiles in directional solidification: Expansion and matching methods. *J. Cryst. Growth.* **112**, 244–282.
[9] Caroli, B., Caroli, C. & Roulet, B. (1991) Instability of planar solidification fronts. In: C. Godreche (editor), *Solids Far from Equilibrium*, Cambridge University Press, Cambridge, New York, pp. 155–296.
[10] Billia, B. & Trivedi, R. (1993) Pattern formation in crystal growth. In: D. T. J. Hurle (editor), *Handbook of Crystal Growth, Vol. 1: Fundamentals, Part B: Transport and Stability*, Elsevier Science Publishers, Norh-Holland, Amsterdam, pp. 872–1008.
[11] Chen, Y. Q. & Xu, J. J. (2011) Global theory of steady deep-cellular growth in directional solidification, *Phys. Rev. E* **83**, 041601.
[12] Xu, J. J. & Chen, Y. Q. (2011) Global stabilities, selection of steady cellular growth, and origin of side branches in directional solidification. *Phys. Rev. E* **83**, 061605
[13] Saffman, P. G. & Taylor, G. I. (1958) The penetration of a fluid into a porous medium or Hele-Shaw cell containing a more viscous liquid. *Proc. R. Soc. Lond. Ser. A.* **245**, 312–329.
[14] Xu, J. J. (1991) Global instability of viscous fingering in Hele-Shaw Cell (I) – formation of oscillatory fingers *Eur. J. Appl. Math.* **2**, 105–132.
[15] Xu, J. J. (1996) Interfacial instabilities and fingering formation in Hele-Shaw Flow, *IMA J. of Appl. Math.* **57**, 101–135.
[16] Xu, J. J. (1996) Interfacial wave theory for oscillatory finger's formation in a Hele–Shaw cell: A comparison with experiments. *Eur. J. Appl. Math.* **7**, 169–199.
[17] Kruskal, M. & Segur, H. (1991) Asymptotics beyond all orders. *Stud. Appl. Math.* **85**, 129–181.
[18] Chapman, S. J. & Vanden-Broeck, J. M. (2002) Exponential Asymptotics and Capillary Waves. *SIAM J. Appl. Math.* **62** , 1872–1898.
[19] Chapman, S. J. & Vanden-Broeck, J. M. (2006) Exponential asymptotics and gravity waves. *J. Fluid Mech.* **567**, 299–326.
[20] Berry, M. V. (1991) Asymptotics, superasymptotics, hyperasymptotics. In: H. Segur, S. Tanveer & H. Levine (editors), *Asymptotics Beyond All Orders*, NATO ASI Series. Vol. 284, Plenum, Amsterdam, pp. 1–14.
[21] Xu, J. J. (1998) *Interfacial Wave Theory of Pattern Formation: Selection of Dendrite Growth and Viscous Fingering in a Hele–Shaw Flow*, Springer-Verlag, Germany, Heidelberg.
[22] Georgelin, M. & Pocheau, A. (2006) Shape of growth cells in directional solidification. *Phys. Rev. E* **73**, 011604.
[23] Xu, J. J. (1991) Interfacial wave theory of solidication–dendritic pattern formation and selection of tip velocity. *Phys. Rev. A15*, **43**, 930–947.
[24] Xu, J. J. (1996) Generalized needle solutions, interfacial instabilities and pattern formation. *Phys. Rev. E* **53**, 5031–5062.
[25] Chen, Y. Q., Tang, X. X. & Xu, J. J. (2009) 3D Interfacial wave theory of dendritic growth: (I)-(II). *Chin. Phys. B* **18**, 671–685; 686–698.